Climate change, not El Niño, main driver of exceptional drought in highly vulnerable Amazon River Basin

Authors

Ben Clarke, *Grantham Institute, Imperial College London, UK*
Clair Barnes, *Grantham Institute, Imperial College London, UK*
Regina Rodrigues, *Univ. Federal de Santa Catarina, Florianópolis, Brazil*
Mariam Zachariah, *Grantham Institute, Imperial College, London, UK*
Simphiwe Stewart, *Red Cross Red Crescent Climate Centre, the Hague, Netherlands (based in Johannesburg, South Africa)*
Emmanuel Raju, *Department of Public Health, Global Health Section & Copenhagen Centre for Disaster, Copenhagen, Denmark.*
Nick Baumgart, *Red Cross Red Crescent Climate Centre, the Hague, Netherlands (based in Copenhagen, Denmark)*
Dorothy Heinrich, *Red Cross Red Crescent Climate Centre, the Hague, Netherlands (based in Edinburgh, UK)*
Renata Libonati, *Universidade Federal do Rio de Janeiro (UFRJ), Rio de Janeiro, Brazil*
Djacinto Santos, *Universidade Federal do Rio de Janeiro (UFRJ), Rio de Janeiro, Brazil*
Ronaldo Albuquerque, *Universidade Federal do Rio de Janeiro (UFRJ), Rio de Janeiro, Brazil*
Lincoln Muniz Alves, *Instituto Nacional de Pesquisas Espaciais (INPE), São Paulo, Brazil*
Friederike E. L Otto, *Grantham Institute, Imperial College London, UK*

Review authors

Joyce Kimutai, *Grantham Institute, Imperial College London, UK*
Sjoukje Philip, *Royal Netherlands Meteorological Institute (KNMI), De Bilt, The Netherlands*
Sarah Kew, *Royal Netherlands Meteorological Institute (KNMI), De Bilt, The Netherlands*
Juan Bazo, *Red Cross Red Crescent Climate Centre, the Hague, Netherlands (based in Peru)*

Main findings

- Highly vulnerable populations were disproportionately affected by the drought. Small-holder farmers, indigenous-, rural- and river communities across the region were among the most vulnerable due to high poverty rates and their high dependency on agricultural food production, availability of freshwater, and import of goods via rivers.
- Exposure to drought impacts was compounded by historical land, water, and energy management practices including deforestation, destruction of vegetation, fires, biomass burning, corporate farming, cattle ranching and other socio-climate problems which have

decreased the water and moisture retention capacity of the land and thus worsened drought conditions.

- In datasets based on weather records the drought is exceptional, even in today's climate, characterised as a 1 in 100 year event for the meteorological drought (SPI) and approx. a 1 in 50 year event in SPEI. While there is a strong drying trend in the meteorological drought, the trend in agricultural drought is even stronger meaning this agricultural drought would have been extremely rare in a cooler climate.
- We first assess to what extent El Niño is a driver of this trend. El Niño reduced the amount of precipitation in the region by about the same amount as climate change; however, the strong drying trend was almost entirely due to increased global temperatures, so the severity of the drought currently being experienced is largely driven by climate change.
- In order to assess whether and to what extent human-induced climate change was a driver of this drought we combine observations-based data products and climate models and look at the 6 month meteorological (SPI6) drought as well as agricultural drought (SPEI6). We find that the likelihood of the meteorological drought occurring has increased by a factor of 10, while the agricultural drought has become about 30 times more likely.
- Using the US drought monitoring classification system, based on agricultural drought, this means that what is now classified an exceptional drought (D4), would have only been a 'severe drought' (D2) without the effects of climate change, caused by burning fossil fuels and deforestation.
- Unless the world rapidly stops burning fossil fuels and deforestation, these events will become even more common in the future. In a world 2°C warmer than preindustrial an event like this would become even more likely by a further factor of 4 for the agricultural drought (every 10-15 years) and a further factor of 3 for the meteorological drought (every ~30 years).
- While all countries in the affected region have drought management plans, the recent droughts indicate a need to reform policy and better integrate proactive support for forecasts and early warnings, drought contingency plans, sustainable water management practices and infrastructure investment to cope with future, more intense droughts.
- These results highlight that despite 'low confidence' in IPCC projections for drought in the region, increasing water stress driven by human-induced climate change as well as other systemic factors continues to be a major threat for the population and requires urgent efforts for more effective water management strategies, interdisciplinary humanitarian response, and regional cooperation that includes farmers and other stakeholders in the planning.

1 Introduction

In the last few decades, the Amazon region has experienced several extreme hydrological events, some of which are described as 'once in a century.' Periods of rainfall below-normal occurred in 1912, 1926, 1963, 1980, 1983, 1995, 1997, 1998, 2005, and 2010, leading to anomalously low river levels. This, in turn, has heightened the risk and occurrence of fires in the region, with significant consequences for human populations and ecosystems (Marengo & Espinoza, 2016; Marengo et al. 2021).

Since June 2023, the Amazon River Basin (ARB) has received significantly below average rainfall. Initially, the northern half of the basin was most affected by this, but from September the entire basin has experienced a significant moisture deficit. This meteorological drought was further compounded by consistently above-average seasonal (June-November) temperatures, increasing evaporation from the

land surface. This resulted in lower water availability in soils, which is crucial for agricultural practices and ecological health. As of January 2024, large parts of the ARB are in a state of exceptional meteorological, agricultural and ecological drought (WMO, 2016). While drought, in some cases very extreme events, is a key part of the biome's history (Coelho et al., 2012), the frequency of occurrence in recent years (Feldpausch et al., 2016) and the significant impacts of the ongoing event merit further investigation into changing drivers of risk.

The drought has caused the lowest water levels in 120 years, when measurements began, in many of the tributaries in the Amazon River (nature, 2023). The low water levels combined with very high temperatures have large consequences on people and ecosystems depending on these rivers. Many communities in the basin depend on the rivers for transportation, leaving them isolated and thus without access to emergency services and health care. The city of Manaus and more than 20 cities have declared a state of emergency and need to ration drinking water (BBC, 2023).

The large riverine system powers significant portions of the affected countries' energy through hydropower, with Brazil relying on hydro power for 80% of its electricity, Colombia 79%, Venezuela 68%, Ecuador and Peru 55%, and Bolivia 32% (USaids, 2018). The drought is significantly impacting dam capacities and energy output and led to power cuts in the region as early as in June 2023. In addition to the transport disruptions this causes huge economic losses with factories unable to continue production, hitting a population with already high levels of poverty. The drought also hit one of the world's most biodiverse regions. More than 150 dolphins died when lake temperatures reached close to 40C in lake Tefé on the western side of the basin (nature, 2023).

Globally, understanding of the link between impactful drought and anthropogenic climate change is growing but remains challenging. Of the 45 IPCC regions studied by working group 1 of AR6, significant increases in agricultural and ecological droughts were observed in 12 regions since 1950, and a decrease observed in 1. Nonetheless, the evidence in all of these results remains only at low confidence at the regional scale (except for the Mediterranean and western North America), and there are still many more regions in which trends are unclear. This is due to the broad range of drivers of drought, including precipitation patterns, seasonal differences, natural and intraregional variability, the compound nature of many types of droughts, and human factors such as land use and water management practices, as well as data availability and a dearth of attribution studies in regions such as the Amazon. However, given the severe impacts of drought in many parts of the world, understanding these changes, both observed and projected, is crucial to manage the risks going forwards.

Drought in the ARB can be especially impactful. This region contains the largest rainforest in the world, making it a global hotspot of biodiversity and a key part of the global hydrological and carbon cycle. In addition, while relatively sparsely populated, it is still home to around 30 million people across several nations including Brazil, Peru, Colombia, Venezuela, Ecuador and Bolivia. As a result, the region is extremely important for planetary, ecological, and human health alike, underscoring the role of monitoring and managing drought and other extremes in this region. This is recognized across an extensive literature. In 2021, the IPCC reported an observed increase in agricultural and ecological drought in northeast South America, but with low agreement in the sign of change in the other subregions that contain parts of the ARB. In all subregions, there was low confidence in the human contribution to these changes (Masson-Delmotte et al., 2021).

There is an array of drivers of drought in the region, with strong intra-regional variability (Marengo et al. 2021). The ARB is extremely large, making up more than a third of the South American continent by land area, stretching from the high Andes in Peru and Colombia down to low-lying coastal regions

of eastern Brazil, and is largely a tropical climate. Rainforest covers approximately 83% of the basin, and spatial variability of rainfall over the region is partly determined by feedbacks between the land surface and atmosphere (Paredes-Trejo et al., 2021). The timing of wet and dry seasons vary across the basin, with the northern subregion receiving more rainfall during March-May and becoming drier from December-February, while the southern subregion follows the opposite pattern (Marengo, 2004). Seasonal rainfall anomalies are also strongly modulated by both the cycles of the El Niño-Southern Oscillation (ENSO) and the meridional SST gradient in the north Atlantic, affecting moisture flow from the Atlantic (Marengo et al., 2013; Saytamurt et al., 2013).

The influence of ENSO on drought in South America is complex to untangle due to diversity within ENSO events (i.e. variations in spatial patterns, life cycles and other characteristics between events of the same overall magnitude (Capotondi et al., 2015)), interactions with other modes of variability and regions, and changing anthropogenic influences. In general, the occurrence of El Niño is associated with drought in the Amazon, especially for the December-February period (Cai et al., 2020), but correlations are weaker for June-November, the main period of the current drought (Jimenez et al., 2019). Analysis of vegetation health in the Amazonas region found that degradation is strongest during El Niño events driven by rainfall scarcity (Vilanova et al., 2021), and tends to turn the Amazon into a net carbon source (Libonati et al., 2021). El Niño events tend to suppress rainfall in north, east and western Amazonia with specific responses depending on whether the maximum SST warming is located in the eastern or central Pacific (Jiménez-Muñoz et al., 2016).

Several significant droughts have occurred in the ARB in the 21st century: most notably in 2005, 2010, and 2015 (Panisset et al., 2017; Libonati et al., 2021). The 2005 drought occurred in the western and southwestern basin, mainly in the Solimões and Madeira rivers, while the 2010 drought occurred in the northern basin. When it occurred, the 2015 drought was the most widespread and damaging on record in the region, affecting around 80% of the entire area (Libonati et al., 2021). All three events were associated with a confluence of El Niño conditions and warming in the tropical north Atlantic, suggesting that multiple drivers have major influences (Marengo & Espinoza, 2016; Jimenez et al., 2019). However, in 2015, the rainfall deficit was further amplified by extreme temperature anomalies increasing evaporation from the land surface (Jiménez-Muñoz et al., 2016), in turn enhanced by land cover change and anthropogenic forcing (Erfanian et al., 2017).

An attribution study of the 2015 event studied the anthropogenic influence on the water deficit in the northern ARB, which has historically experienced the most severe vegetation impacts (Anderson et al., 2018), from October 2015 to February 2016. This study employed two ensembles of the UK Met Office's HadGEM3-GA6 model; a counterfactual ensemble with only natural forcings, and a factual ensemble with anthropogenic forcing included. This found that the likelihood of a similar event has increased by a factor approximately 4 times (2.7-4.7 times) due to anthropogenic forcing (Ribeiro-Neto et al., 2021).

In 2023, many factors are compounding the intensity of the ongoing drought (Rodrigues, 2023). First, a strong El Niño began in late spring and is likely to persist until at least April 2024. This suppresses rainfall and also increases the chances of fire being used as a tactic to clear forest areas. Second, unusual warming in the North Atlantic is resulting in a northward shift of the Intertropical Convergence Zone (ITCZ), thus drawing rain-bringing cloud bands away from the Amazon (Panisset et al., 2017). Finally, while the rate of deforestation has decreased in the past year, multiple years of heightened deforestation

previously have resulted in a less resilient and drier land surface (Rodrigues, 2023). Moreover, droughts in the northwestern Amazon such as this can be especially devastating to the forest and potentially accelerate a tipping point because the forest there is less resilient to rainfall variability than that in the eastern Amazon, which experiences more variability (Ciemer et al., 2019; Hirota et al., 2021). This is because rainfall variability (intra- and inter-annual fluctuations) adds more heterogeneity to the system, as forests that experience more variability seem to be more resilient, likely due to a training effect after experiencing multiple wet and dry periods (Ciemer et al. 2019).

1.1 Event definition

In this study, we explore the potential role of global warming in this drought. As set out above, there are several other relevant factors worth considering in this case, which ought to be investigated through further work. However, our study timescale is short and there is an exponential complexity of investigating multiple covariates across multiple event definitions. We therefore consider the role of GMST, and include qualitative discussion of the potential role of other key factors.

To characterise the event, we use the standardised precipitation index (SPI) and the standardised precipitation evapotranspiration index (SPEI) over 6-months from June to November 2023, and across the entire ARB. SPEI takes into account both precipitation and potential evapotranspiration (PET) from the land surface, which in turn depends on air temperatures. In doing so, the SPEI provides a proxy for the water availability in the region, which contributes more directly to impacts on agriculture and ecology. Meanwhile, SPI allows us to isolate influences on the precipitation deficit only. Using both SPEI and SPI provides greater insight into the sensitivity of our results to the event definition, with possible implications for water management in the region. It also allows results to be independent of assumptions within a specific index, and thus enhancing robustness in the assessment. Across both metrics, the drought is classified according to the US Drought Monitor (D0 - abnormally dry, D1 - moderate, D2 - severe, D3 - extreme, and D4 - exceptional).

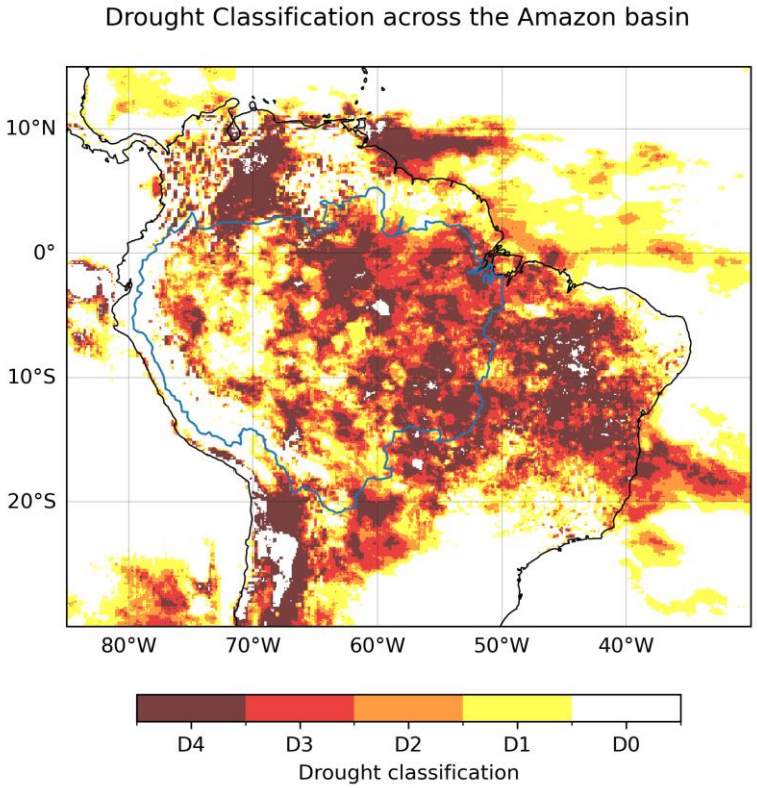

Figure 1: *6-month SPEI (SPEI-6) over the Amazon River Basin (highlighted in blue), from June-November 2023, categorised according to the US Drought Monitor system, calculated from MSWEP and MSWX.*

2 Data and methods

2.1 Observational data

Three gridded observational and reanalysis datasets were used to estimate the severity of the drought in the affected region:

1. The Multi-Source Weighted-Ensemble Precipitation (MSWEP) and Multi-Source Weather (MSWX) datasets, both v2.8 (updated from Beck et al., 2019). These products combine gauge-, satellite-, and reanalysis-based data for reliable precipitation estimates, at 3-hourly intervals from 1979 to near real-time, and at 0.1° spatial resolution globally. The two products are designed to be fully compatible. Here, we use precipitation from MSWEP and minimum and maximum temperatures from MSWX.
2. CHIRPS: Observational daily precipitation dataset developed by the UC Santa Barbara Climate Hazards Group (Climate Hazards Group InfraRed Precipitation with Station data; Funk et al., 2015). Daily data are available at 0.05° resolution from 1981-present. The product incorporates satellite imagery with in-situ station data
3. GPCC Full Data Daily Product Version 2022 of daily global land-surface precipitation totals based on precipitation data provided by national meteorological and hydrological services,

regional and global data collections as well as WMO GTS-data (Ziese et al., 2022). It is provided at a regular latitude/longitude grid with a spatial resolution of 1.0 x 1.0 degree and covers the time period from January 1982 to November 2023. Relative precipitation anomalies at the stations (daily totals divided by monthly total) are interpolated by means of a modified SPHEREMAP scheme (Becker et al., 2013; Schamm et al., 2014; Schneider et al., 2018) and then superimposed on the GPCC Full Data Monthly Version 2022 (Schneider et al., 2022) monthly precipitation totals with climatological infilling.

Initially, the ERA5 reanalysis product (Hersbach et al., 2020) from the European Centre for Medium-Range Weather Forecasts was used to investigate the spatiotemporal extent of the drought, using precipitation, daily maximum and daily minimum temperatures. ERA5 is extensively used in model assessments for the region (e.g. Baker & Spracklen, 2022; Firpo et al., 2022; Olmo et al., 2022). However, comparison across the observational products (ERA5, CHIRPS, MSWEP, MSWX and GPCC) used shows a strong overestimation of the trends in precipitation totals (and SPI) and SPEI (Figs 2a, 3,7). Furthermore, ERA5 characterised the current 6-month drought as much more extreme than other datasets, and suggested the occurrence of droughts over longer timescales (e.g. 24 months shown in Figs A3-A5) that were not recognised by local experts or other datasets. It is included throughout for reference but not as part of the final results synthesis.

As a measure of anthropogenic climate change we use the (low-pass filtered) 4-year smoothed GMST, where GMST is taken from the National Aeronautics and Space Administration (NASA) Goddard Institute for Space Science (GISS) surface temperature analysis (GISTEMP; Hansen et al., 2010; Lenssen et al. 2019).

As a measure of the El Niño - Southern Oscillation cycle (ENSO) we use the detrended Niño3.4 index. This is the Niño3.4 index (average SST over 5° S–5° N, 120°–170° W) minus the SST between 20° S–20° N to adjust the index for climate change, as proposed in Van Oldenborgh et al., 2021. Because we are averaging the index over a period of several months, the values are not standardised per calendar month.

2.2 Model and experiment descriptions

We use two multi-model ensembles from climate modelling experiments using different framings (Philip et al., 2020): regional climate models and coupled global circulation models.

1. Coordinated Regional Climate Downscaling Experiment CORDEX-CORE multi-model ensemble (Gutowski et al., 2016; Giorgi et al., 2021), comprising 18 simulations resulting from pairings of Global Climate Models (GCMs) and Regional Climate Models (RCMs) (12 models at 0.44° resolution (SAM-44) and 6 models at 0.22° resolution (SAM-22)). These simulations are composed of historical simulations up to 2005, and extended to the year 2100 using the RCP8.5 scenario.

2. CMIP6. The ensemble used here consists of simulations from 14 participating models with varying resolutions. For more details on CMIP6, please see Eyring et al., (2016). For all simulations, the period 1850 to 2015 is based on historical simulations, while the SSP5-8.5 scenario is used for the remainder of the 21st century. Past assessments of CMIP6 models show that most are able to reproduce the annual cycle of precipitation in Brazil, though with underestimation in the Amazon, and tend to slightly overestimate temperatures in the Amazon during austral spring (Firpo et al., 2022).

2.3 Statistical methods

We analyse time series of SPI and SPEI values (see sections 3.1.2 and 3.1.3) from the Amazon river basin. Methods for observational and model analysis, model evaluation and synthesis are used according to the World Weather Attribution Protocol, described in Philip et al. (2020), with supporting details found in van Oldenborgh et al. (2021), Ciavarella et al. (2021) and here.

The analysis steps include: (i) estimation of the trend from observations; (ii) model validation; (iii) multi-method multi-model attribution and (iv) synthesis of the attribution statement. We calculate the return periods, Probability Ratio (PR; the factor-change in the event's probability) and change in intensity of the event under study in order to compare the climate of now and the climate of the past, defined respectively by the GMST values of now and of the preindustrial past (1850-1900, based on the Global Warming Index). To statistically model the event under study, we use a normal distribution that shifts linearly with GMST. Next, results from observations and models that pass the validation tests are synthesised into a single attribution statement.

2.3.1 Supplementary methods

The attribution analysis presented in Section 5 and discussed in Section 6, along with much of the observational analysis presented in Section 3, follows the usual WWA protocol: a linear model is used to predict the effect of increasing GMST on drought indices in the Amazon basin. However, in order to understand the contribution of the strong 2023 El Niño event on the drought, we supplement this analysis with a second model that uses both GMST and the detrended Niño3.4 index as covariates, as described in (1) below. In addition, a bivariate model is used to disentangle the contribution to the drought of changes in temperature and precipitation, as described in (2) below. In both of these models, the covariate used is the mean of the detrended Niño3.4 index from June-November: that is, the detrended Niño3.4 index averaged over the same period that the precipitation and PET used to calculate SPI6 and SPEI6 are accumulated over.

1. The variable of interest, X, is assumed to follow a normal distribution in which the location parameter varies with both GMST and the detrended Niño3.4 index, while the variance of the distribution is remains constant, so that

   $$X \sim N(\mu, \sigma \mid \mu_0, \alpha, \beta, T, N), \text{ where } \mu = \mu_0 + \alpha T + \beta N$$

   where X denotes the variable of interest, SPI6 or SPEI6; T is the smoothed GMST, N is the detrended Niño3.4 index, μ and σ are the mean and variance parameters of the nonstationary distribution and α, β are the trends due to GMST and Niño3.4, respectively. As a result, the location of the distribution has a different value in each year, determined by both the GMST and Niño3.4. Maximum likelihood estimation is used to estimate the model parameters.

2. **Analysis of drivers of changing SPEI** - Given the implications of increasing evaporative demand in exacerbating droughts, we supplement the standard univariate analysis of the 6-month SPI in the study regions with an analysis of the joint changes in the 6-month precipitation and PET using copulas, following Zachariah et al., 2023 and Zscheischler and Lehner, 2022).

(i) We fit Gaussian distributions that scale with GMST to the observed 6-month accumulated precipitation (X) and PET (Y) time series respectively:
$X \sim N(\mu_X, \sigma_X \mid \mu_{0X}, \alpha_X, \beta_X, T, N)$ and $Y \sim N(\mu_Y, \sigma_Y \mid \mu_{0Y}, \alpha_Y, \beta_Y, T, N)$.

(ii) We use the cumulative distribution functions (CDFs) of these two distributions to compute the probabilities u and v of exceeding the values observed at each time t, so that
$u_t = P(X \leq x_t)$ and $v_t = 1 - P(Y \leq y_t)$
Note that, because we are interested in the lower tails of the precipitation distribution and the upper tails of the PET distribution, these exceedance probabilities are given by the CDF of X and 1 - the CDF of Y.

(ii) The joint cumulative distribution function C is estimated from the marginal exceedance probabilities u and v by fitting a stationary Student's-t copula such that $C(\{u\}, \{v\}) = P(\{U \leq u\}, \{V \leq v\})$ for all (u, v) pairs (Nelsen, 2006).

(iv) Contours can be plotted over the subset $\{u, v\} \subset \{U, V\}$ - and therefore over the subset $\{x, y\} \subset \{X, Y\}$ - that share the same joint exceedance probability p, where $1/p$ is the return period of the event.

(v) The univariate distributions fitted in Step (i) are used to transform the (u,v) pairs to their equivalent return levels in the current climate, in a 1.2°C cooler climate, and in a climate with a neutral ENSO phase, in order to obtain joint return period contours for the current, pre-industrial and neutral climates.

3 Observational analysis: return period and trend

3.1 Analysis of gridded data

3.1.1 Precipitation and Temperature

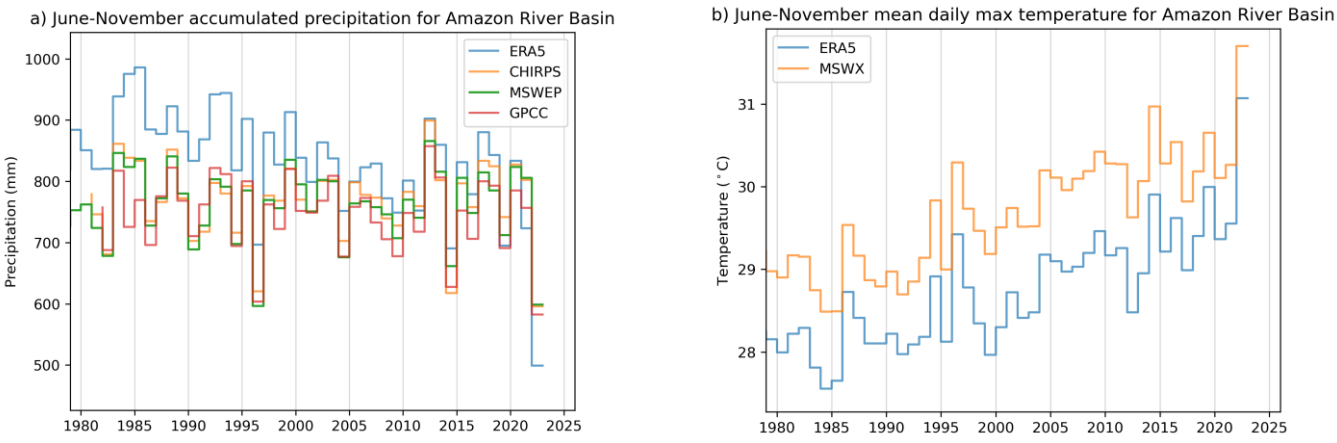

Figure 2: *Observed trends for the Amazon River Basin in a) June-November accumulated precipitation and b) June-November mean of daily maximum temperature, in observational datasets ERA5, CHIRPS, MSWEP/MSWX and GPCC.*

Figure 2 shows observed time series for temperature and accumulated precipitation from June-November of each year on which the SPI and SPEI metrics are based. The time series for MSWEP/MSWX and CHIRPS are available from ~1980 to date, and we use GPCC back to 1982 as a reference dataset. ERA5 is available to 1950 but shows a strong trend in accumulated precipitation not observed in other datasets. Additionally, it returns precipitation deficits of 90-100 mm more than all other datasets for June-November 2023. For these reasons and those set out in section 2.1, it is excluded from our synthesis.

Trends in the mean of daily maximum temperature are consistent across ERA5 and MSWX with a systematic offset of approximately 1 °C. While there are no strong trends in precipitation in datasets other than ERA5, deficits of approximately 200 mm over the 6-month period from June-November 2023 are observed in all datasets. This precipitation anomaly also coincides with a temperature anomaly of around 1 °C above an already strong trend, justifying our analysis of both SPI and SPEI to explore the influence of both rainfall and evaporation on water availability.

3.1.2 SPI

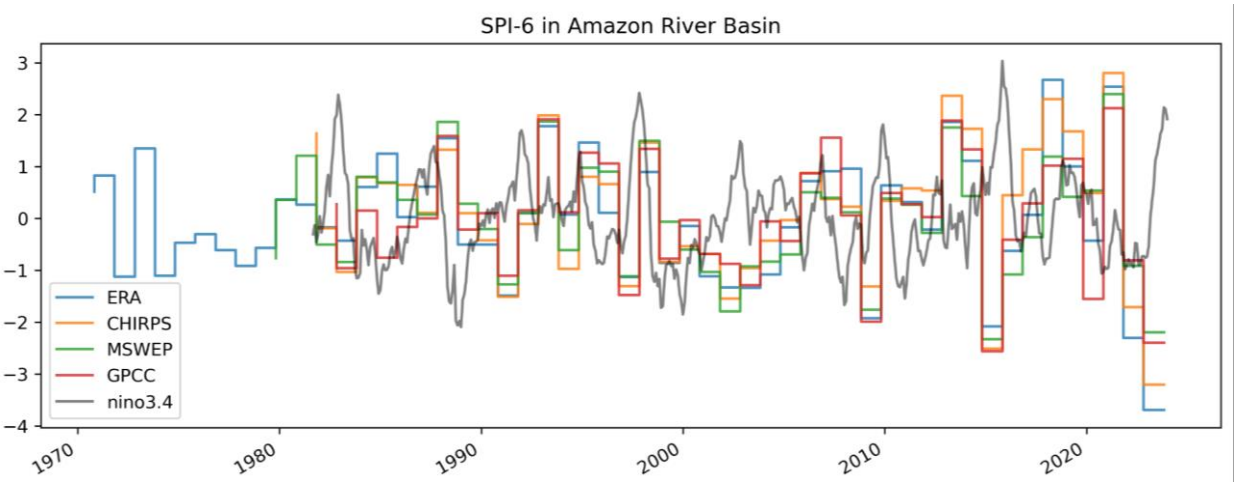

Figure 3: *Time series of observed 6-month SPI from June-November of each year leading up to 2023, in ERA5, CHIRPS, MSWEP and GPCC. The Niño3.4 metric is shown in black.*

Figure 3 shows the observed time series of SPI from June-November each year up to 2023. As expected from the precipitation values in figure 2, SPI displays no trend and increasing variability for most datasets. The last major drought in the region in 2015 is clear as a significant negative anomaly, but others are not clear, likely due to the large spatial extent of the domain used in this figure. The Niño3.4 metric is shown to illustrate the role of El Niño events (positive anomalies in the metric) in basin-wide SPI. As previously stated, the correlation is weak for basin-wide precipitation in the June-November period. We nonetheless test this relationship in section 3.2 since both El Niño and drought had an early onset in 2023. We now present the results of fitting a nonstationary distribution in which the location of the distribution shifts with GMST, as described in Section 2.3, to this time series of June-November SPI derived from the MSWEP, CHIRPS and ERA5 datasets.

Figure 4 shows the time series of SPI in each dataset, with the fitted Gaussian model overlaid. CHIRPS and MSWEP are fairly similar, with very little trend in the mean SPI over time. ERA5, however,

displays a strong drying trend that cannot be ascribed to the longer length of the time series. In all three cases, the mean of the nonstationary distribution (heavy black line) reflects the running mean (blue line) well. According to the Gaussian model fitted to the MSWEP dataset, an increase of 1.2°C in GMST has reduced the SPI by 0.41 (95% confidence interval: -2.41 to 1.57); in MSWEP, by 0.28 (-2.12 to 1.36); and in ERA5, by 2.61 (-4.33 to -0.95). Although both MSWEP and CHIRPS indicate a slight drying trend in the region, the uncertainty about the best estimates is very high, due to a combination of the short length of the datasets included and the high natural variability within the region. As a result the confidence intervals contain zero, and so there is no significant evidence for a reduction in precipitation in this region due to climate change.

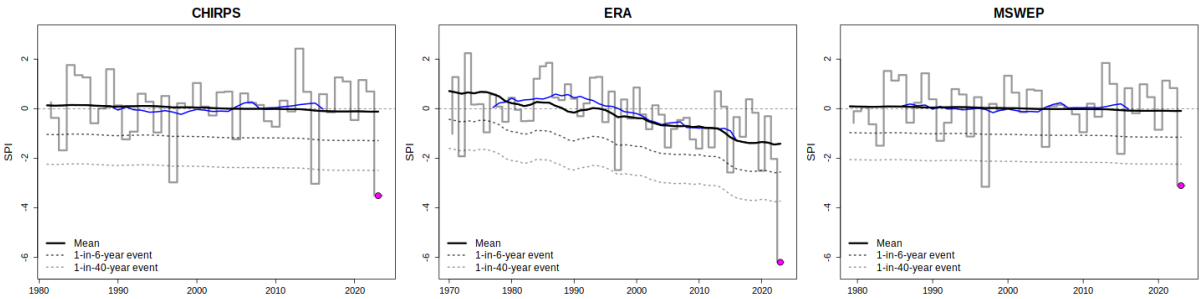

Figure 4: *Time series of observed 6-month SPI over the study region in the CHIRPS, ERA5 and MSWEP datasets. The pink dot marks the 2023 event. The heavy black line indicates the location of the fitted normal distribution, and the dashed lines indicate estimated 6- and 40-year return levels. The blue line is the 15-year rolling mean of the observed time series.*

Figure 5 shows the estimated effective return levels of the observed SPI, transformed to the 2023 climate (in red) and to a cooler climate (in blue). In all three datasets, the Gaussian model fits the data fairly well for moderate events, but more extreme droughts (the lowest SPI values) tend to fall close to the edge of the 95% confidence intervals, or in some cases actually fall outside the interval. Given the known influence of large-scale climate drivers, it is likely that this is due to processes influencing the driest years that are not captured in the statistical model. The effect of adding the Niño3.4 index to the model is explored in Section 3.2; however, GMST-driven trends were not found to be significantly influenced by the inclusion or exclusion of the additional covariate.

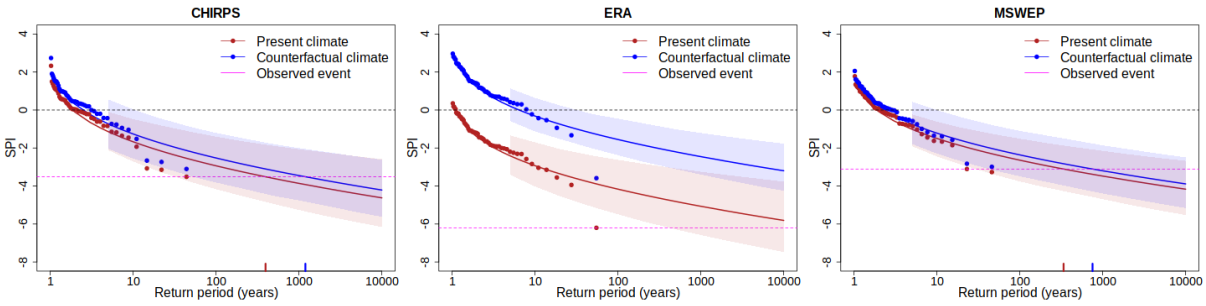

Figure 5: *Expected return levels of 6-month SPI for the 2023 climate (red lines) and a hypothetical 1.2°C cooler climate (blue lines), from the fitted normal distributions. Shaded regions indicate 95% confidence intervals. The pink line indicates the level of the 2023 drought. The estimated return period of the 2023 drought in the current and cooler climates is indicated by red and blue ticks respectively.*

In CHIRPS, the probability ratio is estimated to be 3.0 (95% confidence interval: 0.002 to 924), and in MSWEP, 2.2 (0.05 to 742). In both of these cases, the confidence interval contains one, so although there is evidence of an increased likelihood of severe drought due to climate change, this is not significant. Due to the short length of the time series and high interannual variability, the uncertainty is

high and prevents a strong initial assessment from the observations alone. Due to the strong drying trend in ERA5, the probability ratio is extremely high, with the lower bound of the 95% confidence interval at 289.

The 2023 drought is an extreme event in all three datasets, but in ERA5 the event is much more extreme than in the other datasets. In addition the strong drying trend in this dataset is also markedly different, leading to the decision to exclude ERA5 from further analysis. According to the model fitted to the CHIRPS dataset, events of similar magnitude to the 2023 event are expected to occur once in every 396 years (95% confidence interval: 32 to 1.8 million); in MSWEP once every 337 (31 to 149,000); and in ERA5, once every 39037 years (372 to 28 million). Given the concerns already noted with the ERA5 data, we focus on the return periods from the CHIRPS and MSWEP datasets. Furthermore, due to the relatively poor fit of the statistical model to the most extreme events, it is likely that the estimated return periods are underestimated, and that droughts of this intensity are in fact likely to occur more frequently than once every 300 years: in fact, both MSWEP and CHIRPS have events of similar magnitude occurring within the last forty years. To reflect this fact, we use a return period of 100 years for this event for the attribution analysis.

3.1.3 SPEI

Considering the role of increased PET associated with regional warming in amplifying drought impacts, especially in agriculture due to changes in soil moisture and evapotranspiration rates, we also compute the trends and climate change signals in the 6-month SPEI. As there are several different methods to calculate PET, often with large differences, we first test the sensitivity of SPEI estimates to different methods of calculating PET.

The choice of the PET estimation method in calculating any drought index is subjective but is also limited by the availability of meteorological data and the climatic conditions of the region (Trajkovic et al., 2010; Tabari et al., 2013; Zhao et al., 2021). Several studies (Begueria et al., 2014; Van der Schrier et al., 2011; Dai 2011; Sheffield et al., 2012) have compared and evaluated the effect of using different PET equations in the calculation of drought indices. While most of these studies recommend methods that factor radiative and aerodynamic processes (e.g, FAO Penman–Monteith; Allen et al., 1998) in preference to those that consider temperature as the main input (e.g., Thornthwaite; (Thornthwaite (1948), and Hargreaves-Samani; Hargreaves and Samani, 1985), such methods require several climatic parameters that are often unavailable. We thus only employ temperature based methods: Hargreaves (Hargreaves and Samani, 1982;Hargreaves and Samani, 1985), Baier-Robertson (Baier and Robertson, 1965) and Thornthwaite (Thornthwaite (1948).

To test the sensitivity of the results to the PET-estimation used, spatial fields for the current (June-November 2023) event, and for a longer 24-month event (not shown), are compared to a reference dataset from the Global Drought Crops Monitor (Vicente-Serrano et al., 2023). This dataset uses the recommended Penman-Monteith formulation of PET based on ERA5 data. As a result, despite not using ERA5 in our final analysis, using it here enables a direct comparison between the PET methods. Similar to previous studies, the Thornthwaite method overestimates the PET resulting in a dry bias (Fig 4). Hargreaves and Baier-Robertson provide comparable estimates, but Hargreaves has a lower mean absolute error for both 6- and 24-months (table 1) and is used for the remainder of this study.

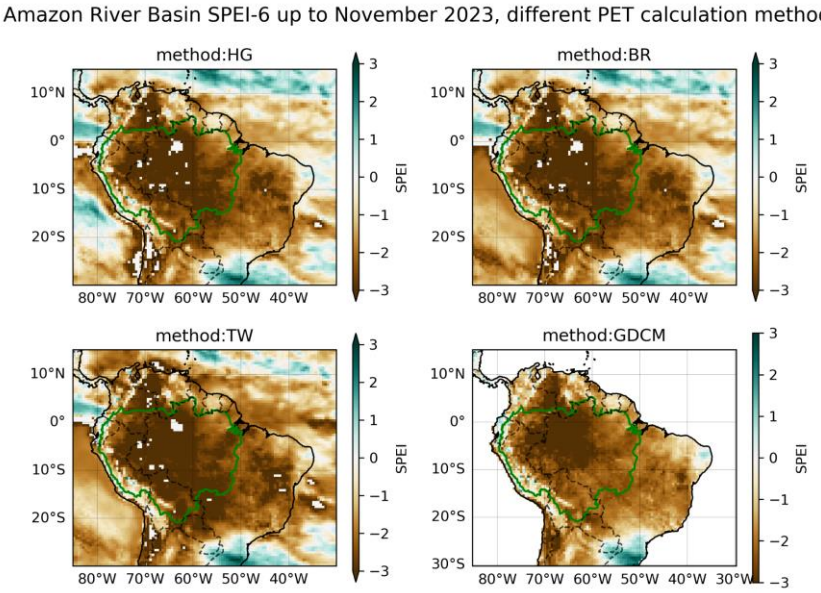

Figure 6: *June-November 2023 SPEI values for the Amazon River Basin using different formulations of PET: Hargreaves (top left), Baier-Robertson (top right), Thornthwaite (lower left), and the Global Drought Crops Monitor using Penman-Monteith (lower right).*

Table 1: *Mean absolute error for each PET estimation method for the current 6- and 24-month drought based on ERA5, measured against the Global Crop Drought Monitor.*

PET estimation method	Mean absolute error	
	SPEI-6	SPEI-24
Hargreaves	-0.41	-0.045
Baier-Robertson	-0.43	-0.081
Thornthwaite	-0.57	-0.163

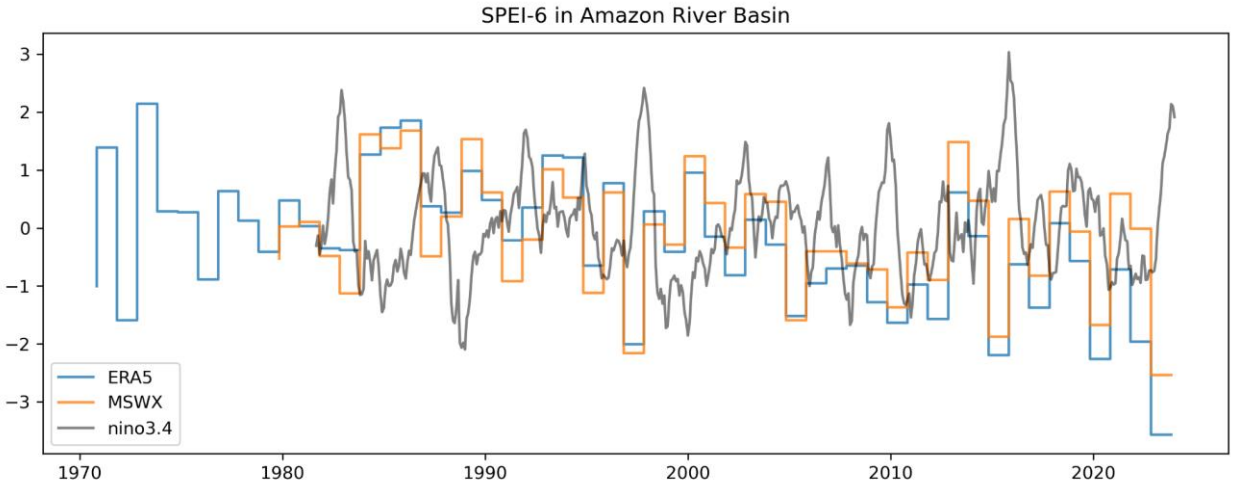

Figure 7: *Time series of observed 6-month SPEI from June-November of each year leading up to 2023, in ERA5 and MSWEP/MSWX. The Niño3.4 metric is shown in black.*

Figure 7 shows the observed time series of SPEI from June-November each year up to 2023. This metric shows a much stronger trend than SPI in both datasets, with Niño3.4 overlaid to show the relationship between El Niño and basin-wide agricultural drought. ERA5 shows a stronger trend and much larger event magnitude than MSWX, but the event is nonetheless exceptional across both datasets. Similar to the analysis for SPI, we present the results of fitting a nonstationary distribution in which the location of the distribution shifts with GMST, as described in Section 2.3, to this time series of June-November SPEI derived from the MSWX and ERA5 datasets.

Figure 8 shows the time series of SPEI in each dataset, with the fitted Gaussian model overlaid. Both ERA5 and MSWEP/MSWX show a decreasing trend in SPEI; again, in both datasets the mean of the fitted distribution (heavy black line) reflects the running mean (blue line) well. According to the model fitted to the ERA5 dataset, an increase of 1.2^{o}C in GMST has reduced the SPI by 2.57 (95% confidence interval: -3.75 to -1.34), and in MSWEP/MSWX, by 1.49 (-3.03 to -0.07). Neither of these confidence intervals contains zero, suggesting that there has been a significant reduction in SPEI in this region due to climate change. However, the difference between the two datasets is smaller when considering SPEI, which takes into account temperature-driven potential evapotranspiration as well as precipitation, than when considering SPI; this suggests that the two datasets exhibit similar trends in warming, and moreover, that this effect dominates the SPEI trend.

The 2023 drought is again an extreme event in both datasets, and more so in ERA5, where events of similar or greater intensity are expected to occur once in every 107 years (95% confidence interval: 27 to 2854); and in MSWEP/MSWX once every 41 years (10-569). Again, it is likely that ERA5 overestimates the rarity of similar events already discussed above; therefore for the remainder of the attribution study we use a return period of 50 years.

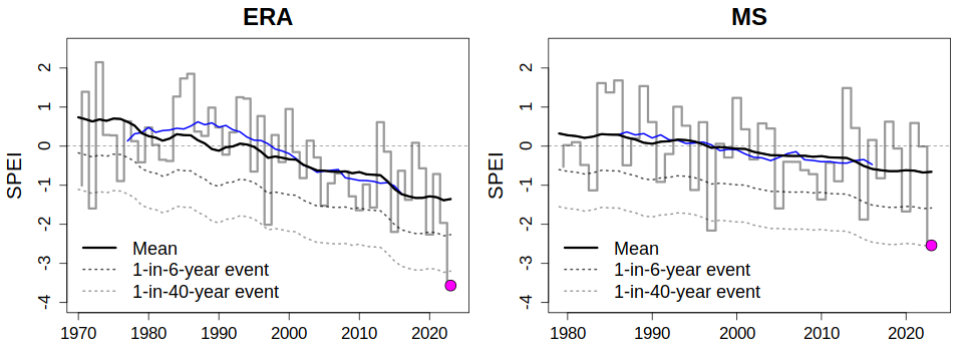

Figure 8: *Time series of observed 6-month SPEI over the study region in the ERA5 and MSWEP/MSWX datasets. The pink dot marks the 2023 event. The heavy black line indicates the location of the fitted normal distribution, and the dashed lines indicate estimated 6- and 40-year return levels. The blue line is the 15-year rolling mean of the observed time series.*

Figure 9 shows the estimated effective return levels of the observed SPEI, transformed to the 2023 climate (in red) and to a cooler climate (in blue). The statistical model fits the SPEI data fairly well even in the tails. In ERA5, the probability ratio is again very high, with a best estimate of 50218 (95% confidence interval: 266 to 456 million), and in MSWEP, 118 (1.25 to 104,000). Again, the uncertainties on the probability ratios are very high: however, both datasets are in agreement that the likelihood of experiencing droughts as extreme as the 2023 event (in the sense of having SPEI values as low as that observed in 2023) has increased significantly.

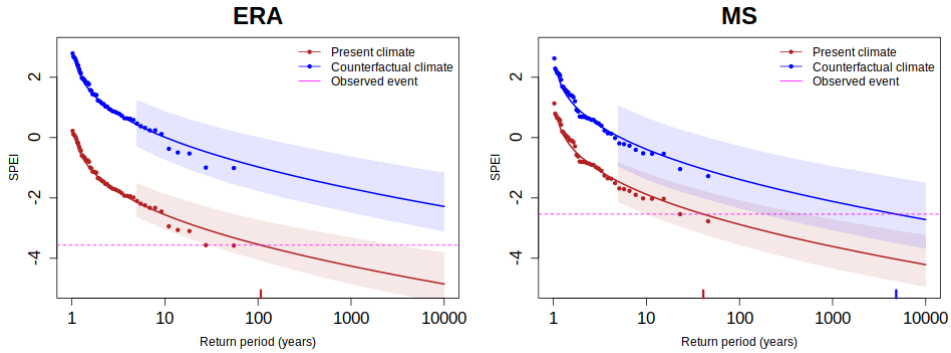

Figure 9: *Expected return levels of 6-month SPEI for the 2023 climate (red lines) and a hypothetical 1.2°C cooler climate (blue lines) in the ERA5 and MSWEP/MSWX datasets. Shaded regions indicate 95% confidence intervals. The pink line indicates the level of the 2023 drought. The estimated return period of the 2023 drought in the current and cooler climates is indicated by red and blue ticks respectively.*

3.2 Influence of modes of natural variability

As noted in the introduction, the 2023 drought may have been influenced by the strong El Niño event that began in late Spring of that year. To test this hypothesis, we extended the statistical model to include the detrended Niño3.4 index (see Section 2.1) as an additional covariate, as described in Section 2.3.1 (1). Figure 10 shows the three SPI time series, with the fitted trend from the original model (as shown in Figure 4) in black, and the fitted trend from the new model in red. A dashed red line has also been added, indicating the location of the distribution when the detrended Niño3.4 index is kept constant at

the 1980-2023 mean level and so isolating the effect of GMST within that model. However, the dashed red line is very difficult to see because it lies almost exactly atop the black line indicating the original model fit, indicating that the estimated GMST trend is almost completely independent of the detrended Niño3.4 index. This is what we would expect to see, given that the Niño3.4 index has been constructed in such a way that the mean trend in GMST has been removed: however, the plots confirm that there is no evidence of any further interaction between the two effects in these datasets.

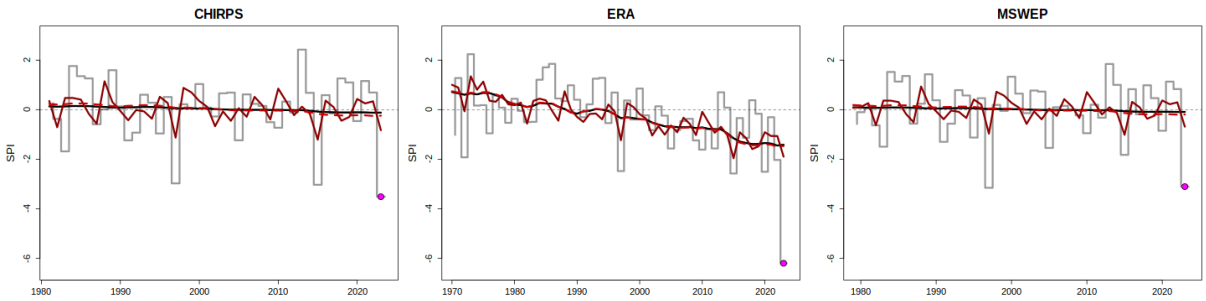

Figure 10: *Time series of observed 6-month SPI over the Amazon basin in the CHIRPS, ERA5 and MSWEP datasets. The pink dot marks the 2023 event. The heavy black line indicates the mean of the fitted distribution using GMST only, and the red line indicates the mean of the fitted distribution using both GMST and detrended Niño3.4 as covariates. The dashed red line indicates the mean of the distribution when the detrended Niño3.4 covariate is keps at the 1980-2023 mean level.*

While the mean trend in SPI is determined largely by the GMST, some of the variability about the mean can be attributed to the Niño3.4 index: in particular, low values of the Niño3.4 index tend to co-occur with low values of the SPI, although the modelled relationship is not strong enough to capture the intensity of the most severe droughts. A similar Niño3.4 effect appears in all three datasets: in comparison with a year with neutral ENSO (that is, Niño3.4 = 0), the SPI was estimated to be reduced in CHIRPS by 0.48 (95% confidence interval: -0.84 to -0.01); in ERA5, by 0.35 (-0.64 to + 0.01); and in MSWEP, by 0.40 (-0.74 to +0.002). The estimated change in SPI due to the current El Niño event is of comparable magnitude to the change due to increased GMST, but with lower uncertainty, so that the effect is found to be statistically significant at the 5% confidence level (Table 2). However, much of the intensity of the 2023 event (which, even excluding the more intense ERA5 event, had an SPI of -3.51 in CHIRPS and -3.11 in MSWEP) remains unexplained by either factor.

Figure 11 shows the 6-month SPI plotted against the observed Niño3.4 values, with the fitted trend overlaid. The 2023 mean of the June-November Niño3.4 index was moderately high but not particularly extreme, and the 2023 SPI would be unusually low under any but the most extreme El Niño; this may arise from natural variability or may suggest that there are additional physical processes affecting the 2023 event that are not captured in the statistical model. There is some evidence of nonlinearity in the rolling mean, suggesting that the linear model used here may slightly underestimate the effect of high values of Niño3.4 on the SPI, although the effect is likely to be relatively small. Due to these uncertainties about the relationship between Niño3.4 and SPI, the known complex and weaker influence of ENSO in the months June-November (as discussed in Section 1), and because we know that the omission of Niño3.4 from the model will not significantly affect the estimated trend in GMST, we only include GMST as a covariate in the full attribution study. This allows the inclusion of several climate models for which estimates of Niño3.4 are not available at the time of writing.

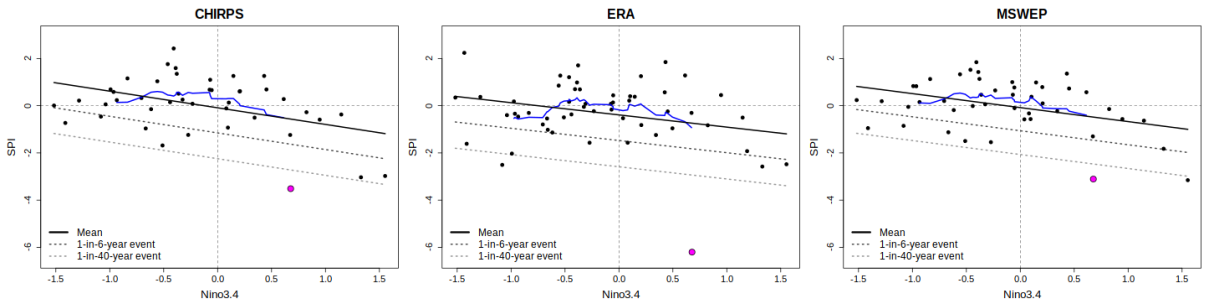

Figure 11: *Observed values of 6-month SPI in the CHIRPS, ERA5 and MSWEP datasets, plotted against the detrended Niño3.4 index, with the GMST held fixed at the mean level. The pink dot marks the 2023 event; the heavy black line indicates the location of the fitted distribution, and the dashed lines indicate estimated 6- and 40-year return levels. The blue line indicates a rolling mean across 15 values of Niño3.4.*

Figure 12 shows the two SPEI time series, with the fitted trend from the original model (as shown in Figure 8) in black, and the fitted trend from the new model in red, and a dashed red line showing the trend due to changes in GMST alone. As in Figure 10, the dashed red line coincides almost exactly with the black line, indicating that, as we would expect, the addition of the detrended Niño3.4 to the model does not affect the estimate of the GMST-driven trend. Again, the modelled effect explains only a small part of the intensity of the 2023 drought, which had an SPEI of -2.54 in MSWEP/MSWX: in comparison with a year with neutral ENSO, the SPEI was estimated to be reduced in ERA5 by 0.23 (95% confidence interval: –0.45 to +0.05) and in MSWEP/MSWX, by 0.24 (-0.53 to +0.07). The estimated change in SPEI due to the current El Niño event is much smaller than the estimated change due to increased GMST (Table 2), and the effect is not found to be statistically significant at the 5% confidence level, although the upper bounds of the interval are only just above zero.

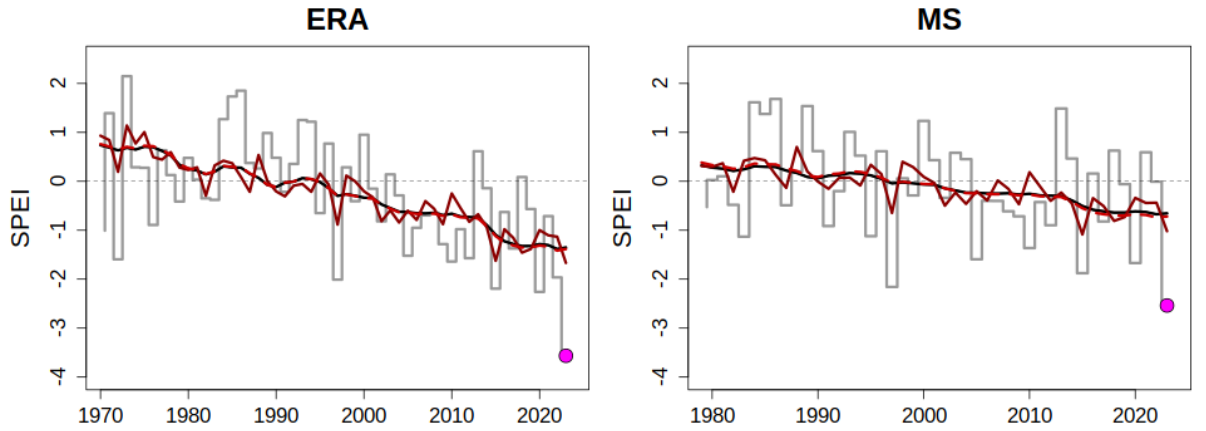

Figure 12: *Time series of observed 6-month SPEI over the Amazon basin in the ERA5 and MSWEP/MSWX datasets. The pink dot marks the 2023 event. The heavy black line indicates the mean of the fitted distribution using GMST only, and the red line indicates the mean of the fitted distribution using both GMST and detrended Niño3.4 as covariates. The dashed red line indicates the mean of the distribution when the detrended Niño3.4 covariate is keps at the 1980-2023 mean level.*

Figure 13 shows the 6-month SPEI plotted against the observed Niño3.4 values, along with the fitted linear trend. The 2023 event is very extreme in ERA5, and even in MSWEP/MSWX it is somewhat unusual given the ENSO conditions: this is probably due to natural variability and unmodelled processes affecting the precipitation, as discussed above.

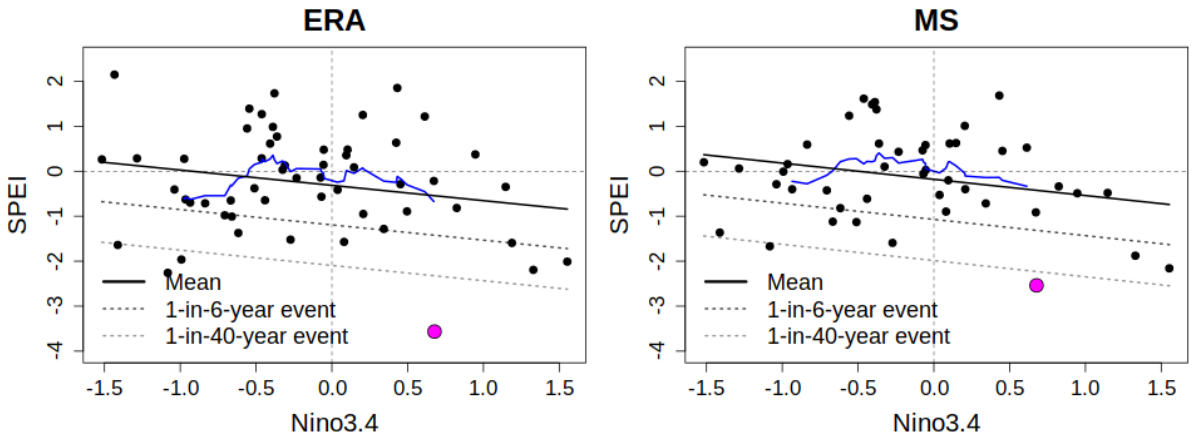

Figure 13: *Observed values of 6-month SPEI in the ERA5 and MSWEP/MSWX datasets, plotted against the detrended Niño3.4 index, with the GMST held fixed at the mean level. The pink dot marks the 2023 event; the heavy black line indicates the location of the fitted distribution, and the dashed lines indicate estimated 6- and 40-year return levels. The blue line indicates a rolling mean across 15 values of Niño3.4.*

The expected changes in SPI and SPEI intensity due to the 2023 value of Niño3.4 are summarised in Table 2, alongside the corresponding changes in intensity due to global warming. It is clear that the effect of ENSO on SPI (and, by extension, on precipitation in the region) is of similar magnitude to that of global warming. For SPEI, even in the more conservative MSWEP/MSWX time series, the effect of increasing GMST has a much larger contribution to the intensity of the drought than the current ENSO phase. We also note that the estimated changes in intensity reported in Sections 3.1 and 3.2 (that is, those obtained from the linear model including only GMST as a covariate), are of slightly smaller magnitude than those in Table 2, implying that this is a conservative modelling choice.

		CHIRPS	**ERA5**	**MSWEP/MSWX**
SPI	GMST	-0.77 (-2.6, 1.29)	-2.71 (-4.27, -1.08)	-0.58 (-2.23, 1.08)
	ENSO	-0.48 (-0.84, -0.01)	-0.35 (-0.64, 0.01)	-0.4 (-0.74, 0.002)
SPEI	GMST		-2.63 (-3.7, -1.42)	-1.68 (-3.18, -0.18)
	ENSO		-0.23 (-0.45, 0.05)	-0.24 (-0.53, 0.07)

Table 2: *Estimated change in SPI and SPEI intensity due to GMST and Niño3.4 in each of the datasets when both GMST and detrended Niño3.4 are included as covariates in the linear model.*

3.3 Drivers of changing SPEI

The discussions in Sections 3.1 and 3.2 highlight the fact that the trends in SPI and SPEI are very different. A 1.2°C increase in GMST increased the precipitation deficit (modelled via the SPI) by roughly the same amount as the 2023 El Niño event; however, the effect of GMST on the water balance (modelled via the SPEI) is much larger than the contribution from ENSO. The reason for this is illustrated in Figure 14, which shows the joint distribution of the 6-month accumulated PET and precipitation over the Amazon basin, along with the corresponding SPEI drought classification for each

pair of values, indicated by the shaded regions. The solid contours indicate pairs of values with the same joint exceedance probability in the current climate: that is, pairs of PET and precipitation values that are equally likely to occur together in 2023. The dashed contours show the equivalent, but for a 1.2°C cooler climate. The magenta circle shows the accumulated precipitation and PET observed in 2023: independent linear models, as described in Section 2.3.1 (1), were fitted to both the precipitation and PET, and used to translate the observed 2023 values into both a 1.2°C cooler climate (turquoise triangle) and a counterfactual climate with a neutral ENSO phase (detrended Niño3.4 = 0) (green square). The change in GMST and the change in Niño3.4 have a similar effect on the magnitude of the precipitation (horizontal shift), which translates into a similar effect on the SPI; however, the change in Niño3.4 has very little effect on the PET (vertical shift), while the change in GMST has a very large effect. This suggests that ENSO acts on droughts in the Amazon basin mainly by reducing precipitation in El Niño years, but has little effect on the temperature and therefore on PET; while increasing the GMST reduces precipitation but also strongly increases local temperatures and PET, which reduces the overall water balance and therefore the SPEI.

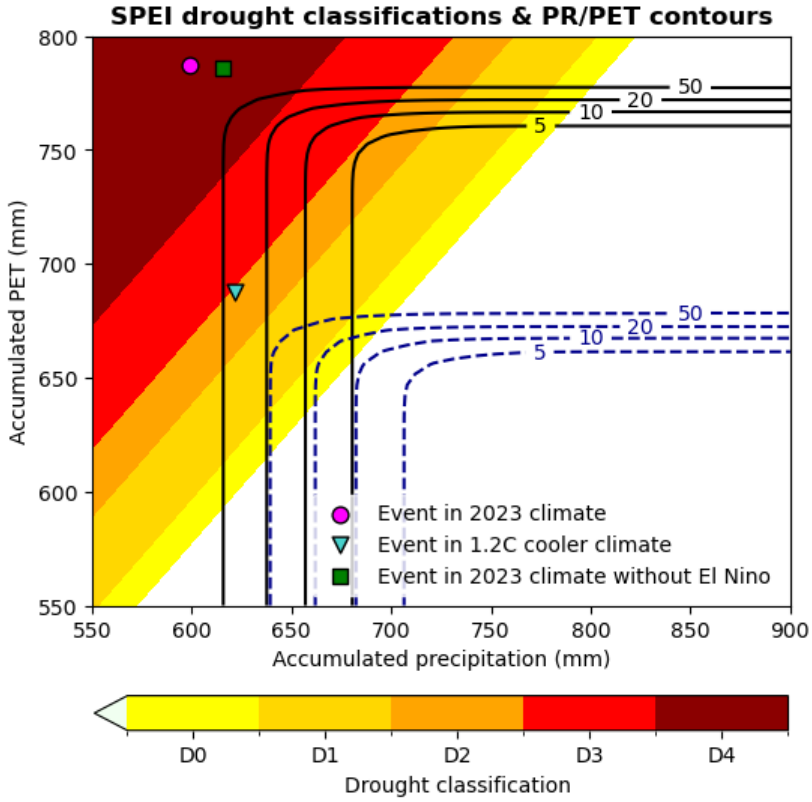

Figure 14: *Joint distribution of 6-month accumulated precipitation and PET with corresponding SPEI drought classification (MSWEP/MSWX dataset). The solid contours indicate return periods under the joint distribution in the current climate, while the dashed contours indicate the same return periods in a 1.2°C cooler climate. The shaded contours represent different levels of drought severity. The magenta circle indicates the 2023 drought in the current climate; the turquoise triangle shows an event of equivalent severity in a 1.2°C cooler climate; and the green square shows an event of equivalent severity in the 2023 climate, but with a neutral ENSO phase.*

4 Model evaluation

In the subsections below we show the results of the model evaluation for 6-month SPI (Table 1) and SPEI (Table 2). The climate models are evaluated against the observations in their ability to capture the

seasonal cycle and spatial pattern of key weather variables, using the MSWEP/MSWX datasets as a reference. For SPI, models are evaluated on how well they capture the seasonal cycle and spatial pattern of precipitation; for SPEI, of precipitation and maximum and minimum temperatures. Taylor diagrams illustrating how well each model captures the shape and amplitude of the seasonal and spatial patterns can be found in Figures A6-A11. Models are also evaluated in terms of how well the statistical distribution of SPI6/SPEI6 matches that of the observational datasets: if the best estimate of the scale parameter falls within the range of values estimated from the observations, the model is deemed 'good'; if the estimated confidence intervals overlap, the model is 'reasonable'; and if the confidence intervals do not overlap, the model is 'bad'. We rate the model as overall 'reasonable' or 'bad', if it is rated 'reasonable' or 'bad', respectively, for at least one criterion. If more than five models are rated 'good' for any framing, we use only the 'good' models in the attribution; otherwise we also include 'reasonable' models. For both SPI and SPEI, both 'good' and 'reasonable' models were included in the attribution analysis.

Table 3: *Evaluation results of the climate models considered for attribution analysis of SPI6. For each model, the best estimate of the scale parameter is shown, along with a 95% confidence interval for each, obtained via bootstrapping. The qualitative evaluation is shown in the right-hand column.*

Model / Observations	**Seasonal cycle**	**Spatial pattern**	**Sigma**	**Conclusion**
CHIRPS			1.21 (0.813 ... 1.48)	
ERA5			1.18 (0.819 ... 1.48)	
MSWEP			1.10 (0.803 ... 1.33)	
CORDEX SAM-22:				
HadGEM2-ES_r1i1p1_RegCM4-7 ()	reasonable	bad	0.980 (0.829 ... 1.08)	bad
HadGEM2-ES_r1i1p1_REMO2015 ()	reasonable	bad	1.05 (0.866 ... 1.18)	bad
MPI-ESM-LR_r1i1p1_REMO2015 ()	reasonable	reasonable	1.28 (0.890 ... 1.56)	bad
MPI-ESM-MR_r1i1p1_RegCM4-7 ()	reasonable	bad	1.10 (0.890 ... 1.25)	bad
NorESM1-M_r1i1p1_RegCM4-7 ()	bad	bad	1.25 (0.981 ... 1.45)	bad
NorESM1-M_r1i1p1_REMO2015 ()	reasonable	reasonable	1.18 (0.888 ... 1.39)	bad
CORDEX SAM-44:				
CanESM2_r1i1p1_RCA4 ()	reasonable	reasonable	0.931 (0.790 ... 1.04)	reasonable
CanESM2_r1i1p1_WRF341I ()	reasonable	reasonable	1.14 (0.936 ... 1.31)	bad
CNRM-CM5_r1i1p1_RCA4 ()	bad	reasonable	0.871 (0.726 ... 0.974)	bad
CSIRO-Mk3-6-0_r1i1p1_RCA4 ()	bad	reasonable	1.06 (0.851 ... 1.23)	bad
EC-EARTH_r12i1p1_RCA4 ()	reasonable	reasonable	0.931 (0.790 ... 1.05)	reasonable
GFDL-ESM2M_r1i1p1_RCA4 ()	reasonable	reasonable	0.935 (0.790 ... 1.04)	reasonable
HadGEM2-ES_r1i1p1_RCA4 ()	reasonable	reasonable	0.922 (0.770 ... 1.05)	reasonable
IPSL-CM5A-MR_r1i1p1_RCA4 ()	reasonable	reasonable	1.26 (1.02 ... 1.43)	bad
MIROC5_r1i1p1_RCA4 ()	reasonable	reasonable	1.04 (0.872 ... 1.17)	reasonable

MPI-ESM-LR_r1i1p1_RCA4 ()	reasonable	reasonable	1.20 (0.985 ... 1.36)	reasonable
MPI-ESM-LR_r1i1p1_REMO2009 ()	reasonable	bad	1.27 (0.997 ... 1.50)	bad
NorESM1-M_r1i1p1_RCA4 ()	reasonable	reasonable	1.11 (0.921 ... 1.24)	reasonable
CMIP6				
ACCESS-CM2_ssp585_r1i1p1f1_gn ()	reasonable	reasonable	0.980 (0.794 ... 1.10)	reasonable
BCC-CSM2-MR_ssp585_r1i1p1f1_gn ()	reasonable	bad	1.13 (0.887 ... 1.33)	bad
CanESM5_ssp585_r1i1p1f1_gn ()	reasonable	bad	1.03 (0.805 ... 1.18)	bad
CMCC-CM2-SR5_ssp585_r1i1p1f1_gn ()	reasonable	bad	0.956 (0.744 ... 1.12)	bad
EC-Earth3_ssp585_r1i1p1f1_gr ()	reasonable	reasonable	0.876 (0.713 ... 0.990)	reasonable
EC-Earth3-Veg-LR_ssp585_r1i1p1f1_gr ()	reasonable	reasonable	0.962 (0.742 ... 1.10)	reasonable
GFDL-CM4_ssp585_r1i1p1f1_gr2 ()	good	good	0.979 (0.737 ... 1.19)	good
GFDL-ESM4_ssp585_r1i1p1f1_gr1 ()	reasonable	reasonable	0.953 (0.783 ... 1.07)	reasonable
IPSL-CM6A-LR_ssp585_r1i1p1f1_gr ()	good	reasonable	0.928 (0.753 ... 1.05)	reasonable
MIROC6_ssp585_r1i1p1f1_gn ()	good	reasonable	0.937 (0.713 ... 1.11)	reasonable
MPI-ESM1-2-HR_ssp585_r1i1p1f1_gn ()	good	reasonable	0.904 (0.685 ... 1.07)	reasonable
MPI-ESM1-2-LR_ssp585_r1i1p1f1_gn ()	reasonable	reasonable	1.11 (0.813 ... 1.35)	reasonable
MRI-ESM2-0_ssp585_r1i1p1f1_gn ()	reasonable	good	0.887 (0.707 ... 1.02)	reasonable
NorESM2-MM_ssp585_r1i1p1f1_gn ()	good	good	1.06 (0.835 ... 1.23)	good

Table 4: *Evaluation results of the climate models considered for attribution analysis of SPEI6. For each model, the best estimate of the scale parameter is shown, along with a 95% confidence interval for each, obtained via bootstrapping. The qualitative evaluation is shown in the right-hand column.*

Model / Observations	**Seasonal cycle**	**Spatial pattern**	**Sigma**	**Conclusion**
ERA5			0.941 (0.753 ... 1.05)	
MSWX			0.956 (0.773 ... 1.08)	
CORDEX SAM-22:				
HadGEM2-ES_r1i1p1_RegCM4-7 ()	bad	bad	0.879 (0.748 ... 0.978)	bad
HadGEM2-ES_r1i1p1_REMO2015 ()	reasonable	bad	0.946 (0.791 ... 1.05)	bad
MPI-ESM-LR_r1i1p1_REMO2015 ()	reasonable	good	1.11 (0.859 ... 1.27)	reasonable
MPI-ESM-MR_r1i1p1_RegCM4-7 ()	reasonable	bad	0.989 (0.816 ... 1.10)	bad
NorESM1-M_r1i1p1_RegCM4-7 ()	bad	bad	1.04 (0.859 ... 1.16)	bad
NorESM1-M_r1i1p1_REMO2015 ()	reasonable	reasonable	1.05 (0.848 ... 1.20)	reasonable
CORDEX SAM-44:				
CanESM2_r1i1p1_RCA4 ()	reasonable	good	0.899 (0.768 ... 0.995)	reasonable
CanESM2_r1i1p1_WRF341I ()	bad	reasonable	1.06 (0.883 ... 1.21)	bad
CNRM-CM5_r1i1p1_RCA4 ()	bad	good	0.854 (0.719 ... 0.957)	bad

CSIRO-Mk3-6-0_r1i1p1_RCA4 ()	bad	good	1.02 (0.828 ... 1.18)	bad
EC-EARTH_r12i1p1_RCA4 ()	bad	good	0.793 (0.663 ... 0.922)	bad
GFDL-ESM2M_r1i1p1_RCA4 ()	bad	reasonable	0.924 (0.774 ... 1.04)	bad
HadGEM2-ES_r1i1p1_RCA4 ()	reasonable	good	0.864 (0.720 ... 0.971)	reasonable
IPSL-CM5A-MR_r1i1p1_RCA4 ()	bad	good	1.19 (0.990 ... 1.34)	bad
MIROC5_r1i1p1_RCA4 ()	good	good	1.02 (0.870 ... 1.13)	good
MPI-ESM-LR_r1i1p1_RCA4 ()	reasonable	good	1.20 (1.01 ... 1.35)	reasonable
MPI-ESM-LR_r1i1p1_REMO2009 ()	reasonable	bad	1.14 (0.921 ... 1.30)	bad
NorESM1-M_r1i1p1_RCA4 ()	bad	reasonable	1.02 (0.865 ... 1.15)	bad
CMIP6:				
ACCESS-CM2_ssp585_r1i1p1f1_gn ()	reasonable	reasonable	0.963 (0.783 ... 1.08)	reasonable
BCC-CSM2-MR_ssp585_r1i1p1f1_gn ()	reasonable	bad	0.913 (0.715 ... 1.04)	bad
CanESM5_ssp585_r1i1p1f1_gn ()	bad	bad	0.949 (0.756 ... 1.08)	bad
CMCC-CM2-SR5_ssp585_r1i1p1f1_gn ()	reasonable	bad	0.939 (0.738 ... 1.09)	bad
EC-Earth3_ssp585_r1i1p1f1_gr ()	reasonable	reasonable	0.868 (0.713 ... 0.977)	reasonable
EC-Earth3-Veg-LR_ssp585_r1i1p1f1_gr ()	reasonable	reasonable	0.976 (0.773 ... 1.10)	reasonable
GFDL-CM4_ssp585_r1i1p1f1_gr2 ()	good	good	0.906 (0.677 ... 1.10)	good
GFDL-ESM4_ssp585_r1i1p1f1_gr1 ()	bad	reasonable	0.928 (0.774 ... 1.02)	bad
IPSL-CM6A-LR_ssp585_r1i1p1f1_gr ()	good	reasonable	0.964 (0.791 ... 1.08)	reasonable
MIROC6_ssp585_r1i1p1f1_gn ()	good	reasonable	0.917 (0.720 ... 1.05)	reasonable
MPI-ESM1-2-HR_ssp585_r1i1p1f1_gn ()	good	reasonable	0.898 (0.687 ... 1.05)	reasonable
MPI-ESM1-2-LR_ssp585_r1i1p1f1_gn ()	reasonable	reasonable	1.08 (0.832 ... 1.26)	reasonable
MRI-ESM2-0_ssp585_r1i1p1f1_gn ()	reasonable	good	0.904 (0.737 ... 1.02)	reasonable
NorESM2-MM_ssp585_r1i1p1f1_gn ()	good	good	0.939 (0.755 ... 1.08)	good

5 Multi-method multi-model attribution

Tables 3 and 4 show probability ratios (PR) and changes in intensity (ΔI) for the observational datasets and for those models that passed evaluation for, respectively, SPI6 and SPEI6

Table 5: *Expected magnitude of a 100-year SPI6 event, along with the probability ratio and change in intensity: (a) from preindustrial climate to the present and (b) from the present to 2C above preindustrial.*

		(a) -1.2C vs present		(b) Present vs +0.8C	
Model / Observations	**100-year event**	**Probability ratio PR**	**Change in intensity ΔI**	**Probability ratio PR**	**Change in intensity ΔI**
CHIRPS	-3.5	3.02 (0.0019 ... 924)	-0.41 (-2.4 ... 1.6)		
ERA5	-6.2	134977 (290 ... 174447610)	-2.6 (-4.3 ... -0.95)		

MSWEP	-3.1	2.24 (0.0054 ... 742)	-0.28 (-2.1 ... 1.4)		
CanESM2_r1i1p1_RCA4	-3.1	18.4 (4.4 ... 103)	-0.88 (-1.3 ... -0.43)	4.2 (2.9 ... 7.2)	-0.54 (-0.69 ... -0.39)
EC-EARTH_r12i1p1_RCA4	-2.2	1.55 (0.32 ... 8.9)	-0.15 (-0.67 ... 0.43)	2.3 (1.3 ... 4.5)	-0.43 (-0.71 ... -0.12)
GFDL-ESM2M_r1i1p1_RCA4	-2.5	17.9 (1.35 ... 413)	-0.87 (-1.7 ... -0.082)	3.2 (1.7 ... 6.4)	-0.48 (-0.76 ... -0.19)
HadGEM2-ES_r1i1p1_RCA4	-3.1	42 (5.85 ... 568)	-1.1 (-1.6 ... -0.49)	1.4 (0.77 ... 2.5)	-0.11 (-0.31 ... 0.085)
MIROC5_r1i1p1_RCA4	-2.7	7.46 (0.79 ... 72)	-0.70 (-1.5 ... 0.081)	1.9 (0.99 ... 3.9)	-0.23 (-0.48 ... 0.0018)
MPI-ESM-LR_r1i1p1_RCA4	-3.3	3.90 (0.39 ... 39)	-0.57 (-1.5 ... 0.29)	1.5 (0.76 ... 2.8)	-0.18 (-0.47 ... 0.11)
NorESM1-M_r1i1p1_RCA4	-2.9	2.75 (0.21 ... 32)	-0.40 (-1.4 ... 0.55)	0.81 (0.33 ... 1.6)	0.078 (-0.18 ... 0.33)
ACCESS-CM2_r1i1p1f1_gn	-2.4	10.1 (1.28 ... 60)	-0.60 (-1.1 ... -0.047)	1.9 (1.1 ... 2.8)	-0.17 (-0.31 ... -0.029)
EC-Earth3_r1i1p1f1_gr	-3.3	20 (6.61 ... 75)	-0.90 (-1.3 ... -0.52)	5.0 (3.8 ... 7.3)	-0.67 (-0.81 ... -0.53)
EC-Earth3-Veg-LR_r1i1p1f1_gr	-2.3	5.04 (1.21 ... 24)	-0.52 (-0.93 ... -0.067)	1.9 (1.2 ... 3.0)	-0.22 (-0.38 ... -0.061)
GFDL-CM4_r1i1p1f1_gr2	-3.4	966 (99 ... 17365)	-1.9 (-2.5 ... -1.2)	15 (9.8 ... 26)	-1.2 (-1.3 ... -0.99)
GFDL-ESM4_r1i1p1f1_gr1	-3.2	201 (18 ... 8466)	-1.6 (-2.3 ... -0.85)	11 (6.4 ... 21)	-1.2 (-1.5 ... -0.93)
IPSL-CM6A-LR_r1i1p1f1_gr	-2.1	4.00 (1.38 ... 13)	-0.40 (-0.75 ... -0.082)	1.4 (0.87 ... 2.2)	-0.11 (-0.28 ... 0.041)
MIROC6_r1i1p1f1_gn	-2.2	28 (1.91 ... 401)	-0.82 (-1.5 ... -0.15)	3.1 (1.7 ... 5.4)	-0.35 (-0.57 ... -0.15)
MPI-ESM1-2-HR_r1i1p1f1_gn	-2.4	3.03 (0.64 ... 11.7)	-0.36 (-0.78 ... 0.15)	2.7 (1.8 ... 3.6)	-0.52 (-0.76 ... -0.25)
MPI-ESM1-2-LR_r1i1p1f1_gn	-3.6	6.13 (1.30 ... 35)	-0.80 (-1.4 ... -0.12)	3.9 (2.7 ... 6.1)	-0.85 (-1.1 ... -0.56)
MRI-ESM2-0_r1i1p1f1_gn	-3.2	96 (21 ... 485)	-1.4 (-1.9 ... -0.93)	5.9 (3.8 ... 10)	-0.74 (-0.96 ... -0.53)
NorESM2-MM_r1i1p1f1_gn	-3.7	657 (64 ... 12232)	-1.9 (-2.6 ... -1.2)	8.1 (4.9 ... 15)	-0.84 (-1.1 ... -0.61)

Table 6: *Expected magnitude of a 100-year SPI6 event, along with the probability ratio and change in intensity: (a) from preindustrial climate to the present and (b) from the present to 2C above preindustrial.*

		(a) -1.2C vs present		(b) Present vs +0.8C	
Model / Observations	**50-year event**	**Probability ratio PR**	**Change in intensity ΔI**	**Probability ratio PR**	**Change in intensity ΔI**
ERA5	-3.57	50218 (266 ... 456069628)	-2.57 (-3.75 ... -1.34)		
MSWX	-2.54	118 (1.25 ... 104820)	-1.49 (-3.03 ... -0.069)		
MPI-ESM-LR_r1i1p1_REMO2015	-3.0	15.9 (1.20 ... 692)	-1.1 (-2.1 ... -0.078)	4.9 (2.8 ... 9.9)	-0.84 (-1.1 ... -0.54)
NorESM1-M_r1i1p1_REMO2015	-3.2	216 (13.5 ... 6487)	-1.8 (-2.8 ... -0.81)	7.1 (3.6 ... 19)	-0.94 (-1.2 ... -0.63)
CanESM2_r1i1p1_RCA4	-3.0	44.5 (11.0 ... 332)	-1.1 (-1.5 ... -0.70)	6.0 (4.0 ... 11)	-0.70 (-0.83 ... -0.57)
HadGEM2-ES_r1i1p1_RCA4	-2.9	109 (18.7 ... 1418)	-1.3 (-1.8 ... -0.80)	2.5 (1.5 ... 4.5)	-0.32 (-0.50 ... -0.14)
MIROC5_r1i1p1_RCA4	-2.6	24.5 (3.23 ... 273)	-1.1 (-1.9 ... -0.40)	3.8 (2.2 ... 7.4)	-0.54 (-0.78 ... -0.31)
MPI-ESM-LR_r1i1p1_RCA4	-3.2	10.3 (1.58 ... 138)	-1.0 (-1.9 ... -0.18)	3.0 (1.8 ... 5.6)	-0.58 (-0.88 ... -0.30)
ACCESS-CM2_r1i1p1f1_gn	-2.4	9.94 (1.64 ... 46.5)	-0.66 (-1.2 ... -0.12)	2.4 (1.7 ... 3.4)	-0.28 (-0.40 ... -0.15)
EC-Earth3_r1i1p1f1_gr	-3.2	21.0 (7.42 ... 69.9)	-1.0 (-1.4 ... -0.61)	4.9 (3.7 ... 6.9)	-0.71 (-0.83 ... -0.59)
EC-Earth3-Veg-LR_r1i1p1f1_gr	-2.2	6.78 (1.76 ... 32.1)	-0.66 (-1.1 ... -0.18)	2.3 (1.5 ... 3.6)	-0.34 (-0.51 ... -0.16)
GFDL-CM4_r1i1p1f1_gr2	-3.3	394 (60.2 ... 3353)	-1.9 (-2.5 ... -1.3)	12 (8.3 ... 20)	-1.1 (-1.2 ... -0.99)
IPSL-CM6A-LR_r1i1p1f1_gr	-2.1	6.85 (2.54 ... 20.8)	-0.60 (-0.98 ... -0.28)	2.1 (1.4 ... 2.9)	-0.27 (-0.43 ... -0.12)
MIROC6_r1i1p1f1_gn	-2.1	27.6 (2.72 ... 305)	-0.90 (-1.5 ... -0.26)	3.8 (2.5 ... 5.9)	-0.47 (-0.66 ... -0.29)
MPI-ESM1-2-HR_r1i1p1f1_gn	-2.2	4.70 (1.09 ... 16.92)	-0.52 (-0.93 ... -0.029)	3.0 (2.2 ... 4.0)	-0.57 (-0.77 ... -0.35)
MPI-ESM1-2-LR_r1i1p1f1_gn	-3.4	6.17 (1.63 ... 48.7)	-0.91 (-1.6 ... -0.25)	2.7 (1.7 ... 4.7)	-0.66 (-0.99 ... -0.36)
MRI-ESM2-0_r1i1p1f1_gn	-3.0	144 (31.1 ... 788)	-1.5 (-2.0 ... -1.1)	6.5 (4.3 ... 11)	-0.81 (-1.0 ... -0.62)
NorESM2-MM_r1i1p1f1_gn	-3.2	825 (114 ... 12387)	-2.0 (-2.6 ... -1.4)	11 (7.1 ... 18)	-1.0 (-1.2 ... -0.81)

6 Hazard synthesis

For the event definitions described above, SPI6 and SPEI6, we evaluate the influence of anthropogenic climate change on the thus characterised drought by calculating the probability ratio as well as the change in intensity using observations and climate models. Models which do not pass the validation tests described above are excluded from the analysis. We also exclude the ERA5 reanalysis. As a point of note, it is imperative to exercise caution when interpreting the ERA results in this region, as precipitation data from reanalyses consistently exhibits extremes that may deviate significantly from observational databases (Lavers et al, 2022). The aim is to synthesise results from models that pass the

evaluation along with the observations-based products, to give an overarching attribution statement. Figs. 15 and 16 show the changes in probability and intensity for the observation-based products (blue) and models (red). To combine them into a synthesised assessment, the following procedure is taken. First, a representation error is added (in quadrature) to the observations, to account for the difference between observations-based datasets that cannot be explained by natural variability. This is shown in these figures as white boxes around the light blue bars. The dark blue bar shows the average over the observation-based products. Next, a term to account for intermodel spread is added (in quadrature) to the natural variability of the models. This is shown in the figures as white boxes around the light red bars. The dark red bar shows the model average, consisting of a weighted mean using the (uncorrelated) uncertainties due to natural variability plus the term representing intermodel spread (i.e., the inverse square of the white bars). Observation-based products and models are combined into a single result in two ways. Firstly, we neglect common model uncertainties beyond the intermodel spread that is depicted by the model average, and compute the weighted average of models (dark red bar) and observations (dark blue bar): this is indicated by the magenta bar. As, due to common model uncertainties, model uncertainty can be larger than the intermodel spread, secondly, we also show the more conservative estimate of an unweighted, direct average of observations (dark red bar) and models (dark blue bar) contributing 50% each, indicated by the white box around the magenta bar in the synthesis figures.

As ERA5 shows a much stronger trend than the other observation based products, and no reason is known why ERA5 could be trusted more, we exclude ERA5 from the quantitative synthesis. This results in an increase in probability (PR) of 11.2 (0.64 to 180) for SPI6 (fig. 15a) which corresponds to an intensity change of -0.78 (-1.53 to -0.037). In other words, a drought classified with SPI6 of -3.11 in the MSWEP observations would have had an SPI6 value of -2.33 (-1.58 to 3.073) in a 1.2C cooler world (fig 15b). For SPEI, again excluding ERA5, the probability has increased by a factor of 36.6 (3.5 to 451) (fig. 16a), and the intensity by -1.17 (-1.82 to -0.52) (fig. 16b). For the drought classified as exceptional today in SPEI6 with -2.54 (MSWEX), drought category D4, this means the drought would only be classified as severe -1.37 (D2) (-0.72 to -2.02) in a 1.2C cooler climate.

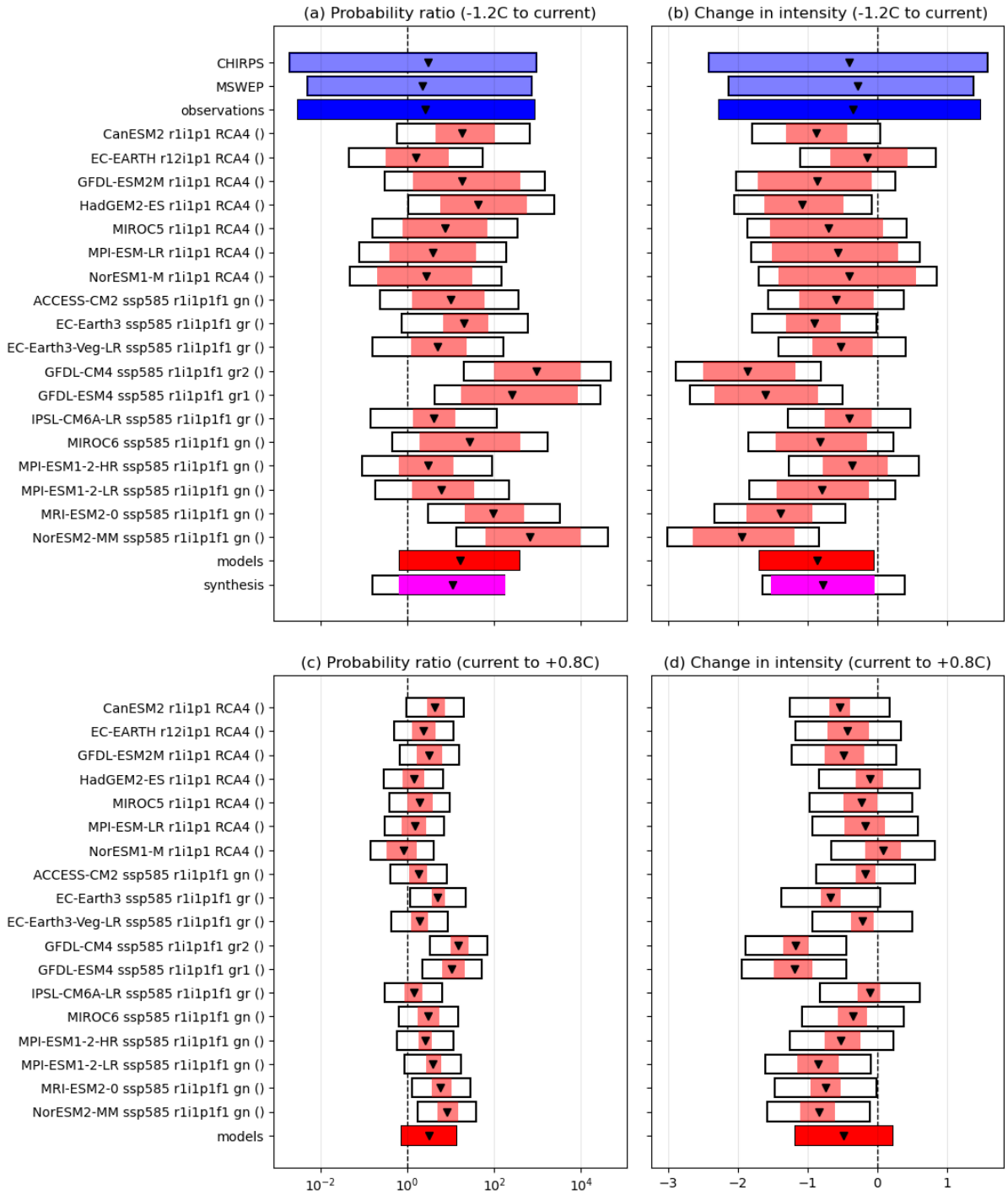

Figure 15: *Synthesis of (left) probability ratios and (right) relative intensity changes when comparing the return period and magnitudes of SPI6 in the ARB: (top) between the current climate and a 1.2C cooler climate and (bottom) between the current climate and a 0.8C warmer climate (ie. with total warming of 2C).*

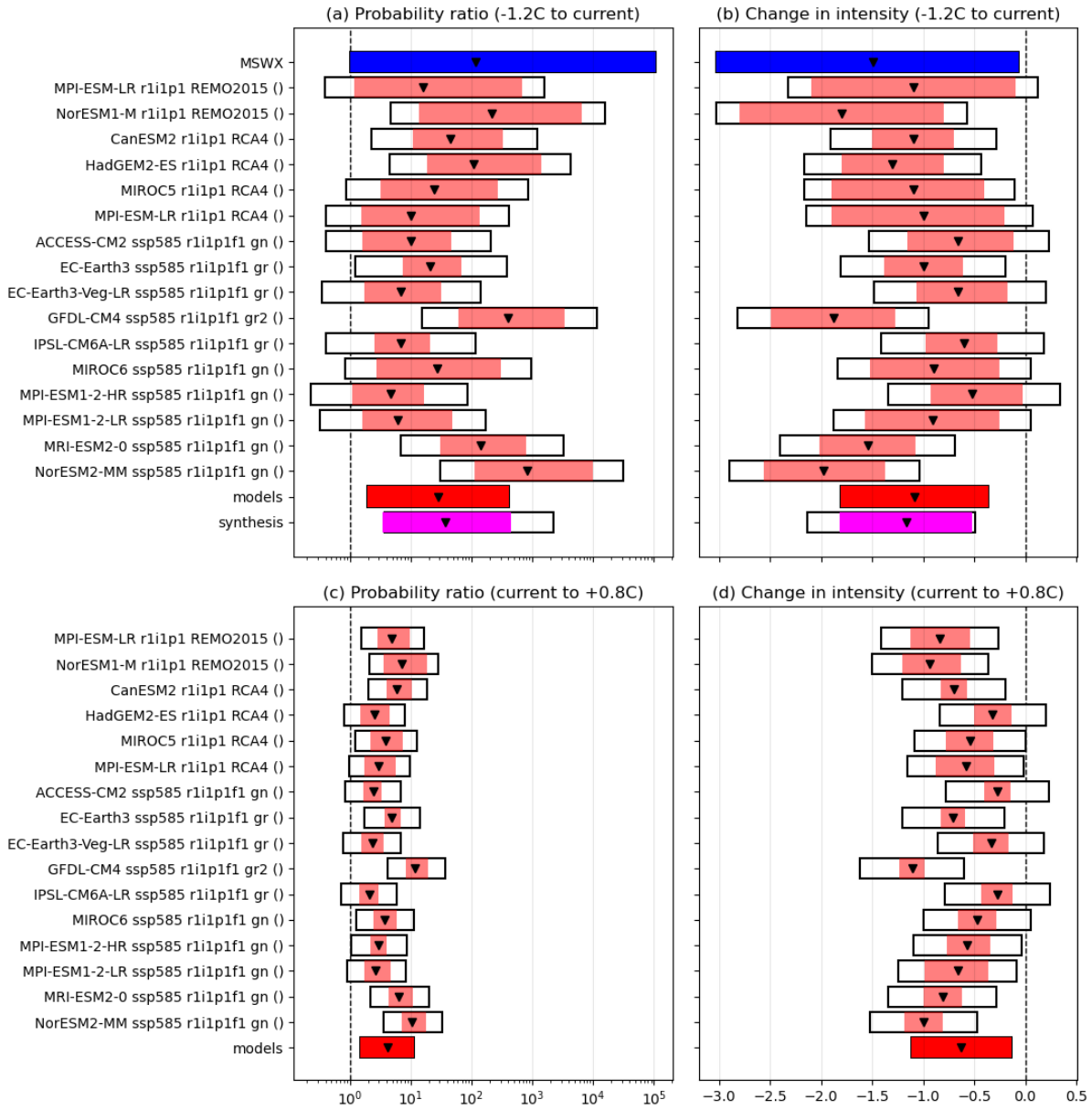

Figure 16: *As figure 15 but for SPEI6.*

The models and observation based products, with the exception of ERA5, are very similar apart from the larger uncertainties in the observations, which is due mainly to the shorter length of these time series. All show the same changes qualitatively and with respect to the order of magnitude. We therefore use the weighted averages, shown as magenta boxes. The observed and model changes are further corroborated by estimating for the same event definitions and models the PR and intensity changes in a 0.8C warmer world from today, which show an increase in likelihood of 3.13 (0.73 - 13.4) for SPI6 and 4.13 (1.51 to 11.3) for SPEI6. The change in intensity is a further -0.67 (-1.12 to -0.14) for SPEI6 and -0.48 (-1.18 to 0.22) for SPI6. This implies that the current trend is indeed driven by anthropogenic climate change.

Combining these lines of evidence from the synthesis results of the past climate, results from future projections and physical knowledge, we communicate the rounded best estimate as the overarching result of our assessment.

7 Vulnerability and exposure

Introduction

In a statement by the United Nations Sustainable Development Solutions Network, the 2023 Amazon drought is described as both unprecedented and unforeseen (2023). While the current drought is the most extreme on the historical record and unique due to its timing (commencing during the pre-rainy season), it is not an isolated case in relation to the exposure and vulnerability pathways highlighted by previous (severe) droughts in the Amazon - including in 2005, 2010, 2015/2016, and 2020 (ibid, 2023). Indeed, the 2023 amazon drought comes at a time when the region has experienced myriad challenges including climate and extreme weather events (Souza da Silva et al, 2023), socio-economic political, and conflict-related challenges (Council on Foreign Relations, 2023; ICRC, 2022). These factors have combined to create a widespread crisis - showing the distinct vulnerability of the Amazon and its people to the impacts of concurrent fragility and climate change. Understanding this dynamic context of V&E can support transformation in preparedness, anticipatory action, and adaptation measures at all levels. This section therefore examines the key V&E factors of the 2023 Amazon drought in order to position the drought in its full context. It considers chronic and differential vulnerability, physical systems (energy, water, land and infrastructure), the discreet interests of households and communities, as well as the policy and humanitarian implications of the 2023 Amazon drought.

Chronic and differential vulnerability

The drought affected amazon region presents geographically diverse micro-climates and differences in socio-political situations of individual countries, resulting in differential vulnerabilities of specific population groups. The varying microclimates expose communities to compounding events of additional extreme heat e.g in Bolivia (IFRC, 2023) wildfires in Brazil (Unicef, 2023), or extreme hail storms in Peru (Save the Children, 2023). Yet, the affected regions share vulnerabilities to a certain degree. Small-holder farmers, indigenous-, rural- and river communities are among the most vulnerable populations to drought in the region due to their high dependency on agricultural food production, availability of freshwater, import of goods via rivers and high poverty rates (OCHA, 2023). Indigenous populations of the Amazon belong the poorest populations groups with 43% being affected and 24% living in extreme poverty, more than twice as much as non-indigenous counterparts, leaving them among the most vulnerable of all (World Bank, nd). Food security is one of the biggest concerns. 43.2 million people in Latin America experience hunger, and an alarming rate of undernourishment can be noted in recent years particularly in Venezuela and Bolivia, before the current drought event (FAO, 2023). Within vulnerable populations, children are particularly vulnerable to malnutrition, might experience stunting, and be more susceptible to infectious diseases (OCHA, 2023). Furthermore, children and women are at particular risk of domestic violence due to negative coping mechanisms related to heightent insecurities (OCHA, 2023). Lastly, individuals with special needs, elderly and pregnant women experience difficulties seeking needed care during droughts (OCHA, 2023).

Research on drought and the effects on livelihoods in the Amazon mostly considers the Brazilian context (Chaves Michaelsen et al., 2020). Nonetheless, evidence is presented in all affected countries, but differences in quality and quantity might prevail:

Brazil is heavily impacted by the drought event and battling with chronic vulnerabilities. A spatial analysis of vulnerabilities to climate hazards, shows that northern parts are particularly vulnerable considering factors such as socio-economic status, special needs population, migration patterns, access

to health services and more. Among all, poverty had the strongest influence, followed by rural/urban development, (de Loyola Hummell et al., 2016). While the data is from 2005, more recent analyses of the amazon region seem to confirm the picture of existing vulnerabilities (Menezes et al., 2018). The low river levels have led to a reduction of more than 60% of transported goods over the river, including food supplies, medicine and water (European Commission, 2023). This results in severely compromised health services in the amazon state, where services were closed due to lack of water and professional supplies (Unicef, 2023). Hundreds of communities were totally isolated with no access to locomotion along the Rio Negro and its secondary and tertiary tributaries (Unicef, 2023). An analysis of roadless urban centres, highlights the increased vulnerability of these communities. Parry et al., 2017 find that remoteness is closely linked to food security, since agricultural production is reduced during and drought, while chronically high food prices increase significantly during drought. First deaths attributed to malnutrition have been identified in September 2023 and treatment delivery remains a major challenge (Unicef, 2023).

Peru is facing chronic vulnerability due to its high inequalities in the population, high poverty rates, especially among rural and indigenous populations (Instituto Nacional de Estadística e Informática, 2022; OXFAM Peru, 2023). Numerous farming activities in Peru, which are mainly located in the Andes, face risks associated with major drought impacts with cascading risks to food security especially considering high inflation rates (The New Humanitarian, 2023). Peru has the highest food insecurity rates in South America (50%) and 12% of children facing chronic malnutrition, statistics that are likely to have worsened in the past months (FAO, 2022; Peru's statistical institute,2020). Coping strategies are limited as fertiliser and drought resilient crops are becoming more expensive (The New Humanitarian, 2023). Furthermore, trust in climate alerts via text message or farming calendars is low among some farmers (Heikkinen, 2021).

Colombia's drought-stricken Andes and Amazon region are among the most vulnerable regions of climate hazards as a spatial analysis shows, using adapted indicators of the study by de Loyola Hummell et al., 2016. The authors identify poverty and underdevelopment as the main drivers of vulnerability to climate hazards (Roncancio, Cutter and Nardocci, 2020). Almost 50% of the population live below the poverty line and especially rural communities are lacking infrastructure, institutional access, are isolated and require food assistance (USaids, 2012; World Bank, 2021). The farming population in these remote locations are often facing low institutional support since much of the land is held without the legal property rights (World Bank, 2023). Additional challenges arise for the population due to armed conflict which has worsened exposure and vulnerability to climatic events e.g., through increased migration and refugee flows, towards the north in the past years, putting the provinces under pressure and potentially increasing intercommunal tensions among displaced populations affected by drought (IFRC, 2023; Roncancio, Cutter and Nardocci, 2020).

Bolivia's rural population is particularly hit by the drought. Rural communities as well as indigenous populations rely heavily on livestock and agriculture. Rural and indigenous populations are facing high poverty rates, making coping mechanisms such as purchasing seeds, fertiliser, and irrigation systems impossible (IFRC, 2023). A loss of crops and livestock can mean a total loss of livelihood, while food prices surge due to the shortage (IFRC, 2023; World Bank, 2017). Migration remains as one of the few coping mechanisms, exacerbating existing vulnerabilities and leaving for example elderly people with little family support (Brandt, Kaenzig and Lachmuth, 2018; World Bank, 2017). Furthermore, children are taken out of school to provide extra labour, resulting in school closure (IFRC, 2023). Some communities can deal better with droughts due to communal meals and potlucks and some families have the possibility to cultivate food (World Bank, 2017).

Ecuador, much like the other countries, is facing multiple intersecting vulnerabilities, such as high poverty levels among the rural and indigenous population paired with high inflation rates, and overall food insecurity, particularly among children (World Food Programme, 2023). Blackmore et al. (2021) revealed that populations in the impacted Andes are facing up to 10 months of food insecurity in recent years, leaving them with little to no capacity to store food. Moreover, small farm holders in the rural areas have already low access to land and lack ownership (World Bank, 2021). Migration is one of the consequences, adding to the large influx of external migrants in the past year, putting more pressure on certain municipalities (Blackmore et al., 2021;World Food Programme, 2023). On a local scale, research from Tingo Pucará shows rural communities that have developed cooperatives providing credit access or crop storing capacities (Blackmore et al., 2023). It is unclear how common such practices are in other communities.

Venezuela is facing a multitude of humanitarian challenges that leave large parts of the population vulnerable. For example, hyper-inflation combined with high extreme poverty, armed conflict, low access to health, millions migrating out of the country and severe food insecurity (Human Rights Watch, 2023). Food security in particular is reaching crisis levels as food prices have surged by 260% to 555% since 2022, a year with already chronically high food prices and the current situation is likely to worsen (FEWS NET, 2023). Currently, approximately 10.9 million Venezuelans are lacking access to food and studies show that only 9% of households can be considered food secure (Human Rights Watch, 2023;Herrera-Cuenca et al., 2022). Therefore the current drought is placing large parts of the country at risk of hunger, especially children, who are already showing high mortality rates, a trend likely to increase (García, Gerado Correa and Rousset, 2019). Herrera-Cuenca et al., 2022 further reveal that households have to give up their livelihoods to feed their families with 40% of the people spending more than 75% of their income on food.

Water and electricity systems

The Amazon Basin holds a fifth of the world's freshwater resources and its communities and their livelihoods depend on it (USaids, 2018). The large riverine system powers significant portions of the affected countries' energy through hydropower, with Brazil relying on hydrogen power for 80% of its electricity, Colombia 79%, Venezuela 68%, Ecuador and Peru 55%, and Bolivia 32% (USaids, 2018). The drought is significantly impacting dam capacities and energy output. Some Dams are unable to operate like the Madeira dam in Brazil and Venezuela's Guri dam (Bloomberg, 2023; Centre for Climate and Security, 2019). During the 201472015 drought, basins leading up to the dams were impacted significantly and the majority of the dams were operating at the lower end of their capacity even after rainy seasons 2020/21(Cuartas et al., 2022). Venezuela has experienced power cuts already in June 2023, and Ecuador also imposes major power outages lasting several hours a day for the Sierra and Amazon region (Reuters, 2023; Reuters, 2023). In Venezuela, the drought is affecting a deteriorating energy system that has been under stress over the past years due to political instability, lacking regulations and market failures, resulting in irregular energy supply of up to 100 h (Léon-Vielma, Ramos-Real and Hernández, 2022). The coping strategies differ. The Brazilian government has set up diesel power plants, and Ecuador is importing geothermal energy from Colombia, to keep electricity supply at a minimum, however supply remains critical (Bloomberg, 2023; Reuters, 2023). Also Peru has increased energy production through diesel, coal and gas, due to a 15% drop in hydrogen energy output (Peru Support Group, 2023;. Further reduction is to be expected since three of the relevant rivers are affected by the current drought (Cañon del Pato, Mantaro and Urubamba river) (USaids, 2017). Colombia's and Bolivia's energy system appears less impacted by the drought. Bolivia has the

lowest dependency on hydrogen power in the study area and abundant oil and natural gas in its energy mix (IEA, 2023). Colombia's dams were at a high capacity as of August 2023 and water has been saved for the drought (BN Americas, 2023). Moreover, Colombia has large coal reserves and geothermal energy supplies (Reuters, 2023; World Bank, 2021). While no major power restrictions might occur, prices are increasing significantly, the output of the dams has reduced in December and the IEA (2023) has issued a warning that the drought could lead to variability in the energy supply (Rystadt Energy, 2023).

Next to the energy system, water systems have been severely impacted. As much as 77% and 74.8% of the fresh water supply is consumed by the agricultural sectors in Brazil and Peru respectively, leaving many communities and the connected food nets insecure with generally lower access than the urban population (National Water Agency Brazil, 2020; OECD, 2019). In Peru, and Colombia changes in water availability have been linked to increased competition for and even conflict in the past (USaids, 2017; Moncada et al., 2020). In Venezuela, the water system is lacking maintenance and investments, resulting in limited water availability in both urban and rural areas (Moreno-Pizani, 2021). Water security and access have been problematic prior to the drought. In Colombia, 400 municipalities are considered at risk of water shortage meaning one third of the urban population is experiencing water stress (World Bank, 2020).

During the current drought, water scarcity has been reported for river communities and indigenous groups in Brazil and 13 Peruvian regions declared state of water emergency as of December 2023 (Unicef (2023); The New Humanitarian, 2023) Also in Ecuador and Bolivia, water scarcity and low access has forced rural communities to opt for unsafe drinking water since water sources are compromised or kilometres away (Blackmore et al, 2023; IFRC, 2023). In Bolivia's urban areas water has been rationed, drinking water prices have surged and water supply and quality have been diminished, including in schools and hospitals (Reuters, 2023;IFRC, 2023). Also in Venezuela supplies are decreasing at a fast pace and lack of drinking water is a major concern in the capital districts (Think Hazard, 2024; IFRC, 2023; OCHA, 2023). The government response and coping possibilities from communities remain limited. In Brazil for example, over half of the municipalities (62%) do not have emergency measures and communities are dependent on distribution channels or opt for dwells where possible (UNICEF, 2023). The vast majority of the indigenous populations (87%) included in the Unicef survey (2023), did not receive support for drinking water. Although the Peruvian government has established an El Niño mitigation, there are challenges in its implementation. For example, the fund allocates very little to drought conditions in the Andean and none to Amazonian populations (OXFAM, 2023). Vitally, it does not allocate additional for districts in water emergency situations (ibid, 2023).

Land-use changes and environmental degradation

Despite contemporary efforts towards mitigating deforestation, longstanding land use changes across the amazon basin have contributed to vulnerability and exposure pathways across the region including through systems, processes, and policies which exacerbated forest loss throughout the last 40 years (Maeda et al, 2023). Most significantly, a history of deforestation, destruction to vegetation, fires, biomass burning, corporate farming, cattle ranching and other socio-climate problems has decreased the water and moisture retention capacity of the land contributing to cycles of accentuated drought in the region (UNDRR, 2023; Greenpeace, 2022; NASA, 2023). Multiple and synergistic factors such as existing economic and institutional practices, particularly in agriculture and water management, have had distinct consequences for this exposure pathway (Marengo et al, 2018). For example, the agriculture frontier in the amazon continues to expand due to economic and institutional factors such as low internal

cost for land, labor and fuel; increases in the price of products; formal measures which favor deforestation; land use and economic development practices which are associated with transportation expansion, subsidies for land-based activities and; systemic challenges in land use management policy e.g., corruption and mismanagement of the forestry sector also played a key role in driving forest and biodiversity loss (RAISG, 2015). Parts of Peru and Bolivia are particularly at risk as deforestation decreases in Brazil while increasing in these territories where as much as 1,100 miles of Peru's forests are cut down each year and as much as 80 percent of them due to illegal practices (Oxfam, 2021; Praeli, 2021). At the same time, mining, disorganized mineral extraction and fires near river banks contribute to fallen land - when erosion and water action compromise river banks - and grounding of water vessels which jeopardizes navigation and logistics for those villages in the interior of the amazon relying on the river for food and livelihoods in the context of existing shortages and drought (UNDRR, 2023; Souza et al, 2021).

Disputes over land use and land management practices between government and indigenous communities pose further challenges to sustainability in the context of drought. While the rainforest presents a great potential to drive economic development through practices such as mining, plantations, and other extractives; indigenous communities seek to prioritise the conservation of biodiversity for inter-generational cultural practices and food security (Chemnick, 2020). As this conflict of interest increasingly finds purchase in legal and regulatory systems, for example through litigation, it has brought attention to the role of judiciaries in the region to influence sustainable land use and land management e.g., through granting land tenure and ownership rights to indigenous groups (UNHCR, 2022). Recent studies indicate that granting ownership rights to indigenous groups can decrease deforestation by as much as two thirds in the Brazilian Amazon in particular; a sharp contrast to extractives industry and commercialisation (Chemnick, 2020).

Household coping strategies

Communities and households living along and depending on the Amazon's vast networks of waterways and fertile land face disproportionate exposure to the impacts of drought in the region where climate change has contributed to a "record breaking drought" (Rodrigues, 2023). Reports from households in the drought affected region focus on issues of socio-economics, health, and struggles to adapt to the rapidly changing climate (UNICEF, 2023). These reports highlight the dynamics faced by households coping and adapting to drought in the context of existing complex crises.

Across the food and agriculture supply chain, the drought is impacting navigation and the movement of people, goods, and services. In Brazil for example, cash crops such as bananas, cassava, chestnut and acai spoil in the middle of the rainforest as farmers struggle to navigate the network of creeks connecting their metal canoes to markets in the hardest-hit municipalities such as Bom Jesus de Igapo Grande (Hegarty, 2023; Hughes, 2023; Watts, 2023).

Health, humanitarian and emergency response systems are also under increasing pressure, creating cascading impacts for thousands of households. In the Brazilian state of Amazon alone, 100% of municipalities have been in a state of emergency since October 2023 with as many as 150,000 families affected, totalling more than 600,000 people who continue to be inaccessible as river levels remain low e.g, in parts of Rio Negro, Manaus (UNICEF, 2023). Brazil's government has introduced emergency response measures such as supporting affected families through food rotation, personal hygiene kits, sodium hypochlorite distribution, river drainage (to support the movement of boats), renegotiationg debts, promoting rural producers, cash assistance and providing generators for alternative energy supply

(ibid, 2023). However, these measures not only put strain on the government's response capacity as the scale of humanitarian needs far exceeds existing resources but also indicate the total system collapse which widespread drought can exacerbate in the amazon basin.

In parts of Peru, Columbia, and Ecuador the drought has impacted farmers, herders and pastoralists, and children, at a disproportionate rate. According to Peru's Statistics Institute, children are bearing the brunt of the drought as chronic malnutrition and anemia reach record levels. In 2022, 11.7% of children under 5 suffered malnutrition while 42.4% in the same bracket experienced anemia. These statistics are despite Peru being the globe's main producer of crops such as avocados, mangoes, blueberries, table grapes, asparagus, and peppers – an industry which contributes more than 5.7 billion USD to the economy - even during unseasonably hot temperatures caused by El Niño (New Humanitarian, 2023). These disparities drive unsustainable coping practices, patterns of migration and displacement in a context already experiencing fragility. In Colombia for example, the International Committee of the Red Cross (ICRC) reported at least 7 active armed conflicts between the Colombian state and multiple armed groups (IFRC, 2023). Between 2017 - 2022, as many as 168,000 people were forcefully displaced by armed conflict alone. With more than 616,000 people affected by climate change related events in the same period (as of December 2022), the drought is occurring at a time when conflict and climate and extreme weather events have combined to increase widespread vulnerability. In addition to those impacted by armed conflict, floods, landslides and flash floods during the La Niña phenomenon of 2022, the drought finds 5.4 million people (migrants, refugees, returning Colombians and host populations) already in need of humanitarian assistance (IFRC, 2023).

As systemic and environmental factors such as water management, investments in infrastructure development, precipitation deficits, above-average temperatures, and recurrent heat waves cause cascading impacts to water access, households are exposed to the impacts of ongoing drought. In Uruguay, northern Argentina, and southern Brazil they will face distinct challenges resulting from water impacts alone (European Commission, 2023). For example, in Uruguay, combined factors of water management, under-investment in infrastructure, and drought have contributed to 3.5 million people living without access to tap water for drinking by July 2023 (Tocar, 2023). While Uruguay is considered relatively 'high income' by regional standards, households and institutions will have to adopt more and more adaptation measures to cope with drought impacts which previously seemed unlikely including reliance on bottled water for drinking and fiscal policy adjustments to taxation of bottled water consumables as well as prioritized investments in infrastructure and water management (ibid, 2023). These conditions highlight how institutional policy, climate and extreme weather events combine to exacerbate vulnerability across households, communities, and national governments influencing their coping strategies and adaptation options during extreme events.

Drought risk management and policies

Drought risk management tools, policies, and methods can be determinants of the duration and intensity of impacts that are felt during periods of below-average rainfall. The region is no stranger to meteorological droughts and all countries have drought management policies in place to various degrees. At an international level, climate change impacts on drought risks and its management are clearly noted as a concern for the region. Climate change adaptation was included in all the original South American intended nationally determined contributions according to a UNFCCC analysis done in 2016 (Tigre, 2019). Among the South American countries in our event definition, Brazil, Peru, Chile, Columbia, Paraguay, and Uruguay also all have national adaptation plans with the UNFCCC which all

mention drought as a key concern (UNFCCC, n.d.). As recently as 2023, Brazil introduced a suite of Federal actions against drought in Amazonas which amounted to R$ 628 million (Ministry of Environment and Climate Change, 2023). These actions included fire prevention, payments to households living in Conservation units and extractives reserves, dredging, logistics, and medical supplies to affected areas (Ministry of Environment and Climate Change, 2023). Despite these interventions, comprehensive drought management policies at the national level can benefit from anticipation and contingency planning. In a 2017 white paper co-authored by the UN Convention to Combat Desertification, the WMO, and others highlighted the importance of national drought contingency plans in the region which at the time were lacking (UNCCD, 2017).

A significant amount of academic literature has been published about drought management in the region including an extensive overview of drought management in Northeast Brazil by Marengo et al. (2022) who highlight the importance of moving towards holistic and proactive drought management approaches rather than reactive ones. These types of approaches include increasing support for forecasts and early warnings, developing drought contingency plans, prioritizing sustainable water management practices and infrastructure (FAO, 2019). They also include crucial humanitarian response capacity which forms a key part of regional disaster response capacity. For example, the Red Cross Disaster Response Emergency Fund (DREF) - funding released for early action and immediate disaster response - which was triggered in response to the drought in Bolivia and which can also be launched in response to floods, fires, and civil unrest (IFRC, 2023). According to some authors, the current prolonged drought, in fact, led to some policy shifts in this direction. For instance, in a 2023 paper, Cavalcante et al. argue that, in Brazil, the creping drought conditions as well as increased attention from various sectors has triggered a policy change towards more proactive approaches (Cavalcanted et al. 2023).

Finally, national disaster management laws can inscribe drought response mechanisms and require investment. For instance, in Peru, significant investments were made in establishing national disaster management systems through policy reforms in the past 10 years (World Bank, 2021) - in 2017, a study by OPM and WFP showed significant improvements in the social protection system and a strong potential to integrate shock-responsiveness within the different mechanisms (OPM, 20217). In drought response, social protection programmes (such as those providing cash transfers or training) are important tools at the disposal of national or local governments or civil society organizations to support farmers and communities most strongly affected. For example, in Brazil, the Garantia Safra is a public index-based risk insurance programme funded and run by the state and covers over 1 million farmers across the country (numbers from 2016) with a particular focus on smallholder farmers especially in the Northeast (IPCIG, 2020).

V&E conclusions

The 2023 Amazon drought is frequently cited as the most extreme on the historical record. It occurs at a time when communities across the region face distinct and intersecting challenges related to historical drought, recent climate and extreme weather events intensified by the La Niña climate patterns, governance and development challenges, as well as fragility, conflict and violence. The vulnerability and exposure context of the drought highlights the ways in which climate change can exacerbate underlying local, national, and regional challenges resulting in similar vulnerability and exposure outcomes even across seemingly dissimilar contexts. Differences in micro-climate and socio-political systems can produce differential vulnerability to extreme heat, wildfire, and hailstorms e.g., in parts of Bolivia, Brazil, and Peru respectively. However, populations of small-holder farmers, indigenous, rural and river communities across these countries exemplify the extent to which climate and extreme

weather events similarly impact specific sectors across contexts. This dynamic sheds light on the potential for broad based climate action in response to vulnerability. Dependency on agriculture, freshwater, local-global supply chains (of imports and exports), and cash assistance amongst these groups call renewed attention to the need for systemic transformation in anticipation of more intense and frequent climate change events of the future. At the same time, systems, policies, and processes in energy, water and land use management, legislation concerning land tenure and ownership as well as capacity building in national and international humanitarian response suggest that addressing V&E should be a priority in climate action and institutional action in the Amazon basin.

Data availability

Almost all data are available via the Climate Explorer.

Global Crop Drought Monitor data is available at: https://global-drought-crops.csic.es/.
For further information, see:
Vicente-Serrano, S.M., Domínguez-Castro, F., Reig , F., Latorre, B., Beguería, S., SPEICropDroughtMonitor [Dataset], Instituto Pirenaico de Ecología (IPE - CSIC) and Estación Experimental de Aula Dei (EEAD - CSIC), https://doi.org/10.20350/digitalCSIC/15469, 2023.

References

All references are given as hyperlinks in the text.

Supplementary figures

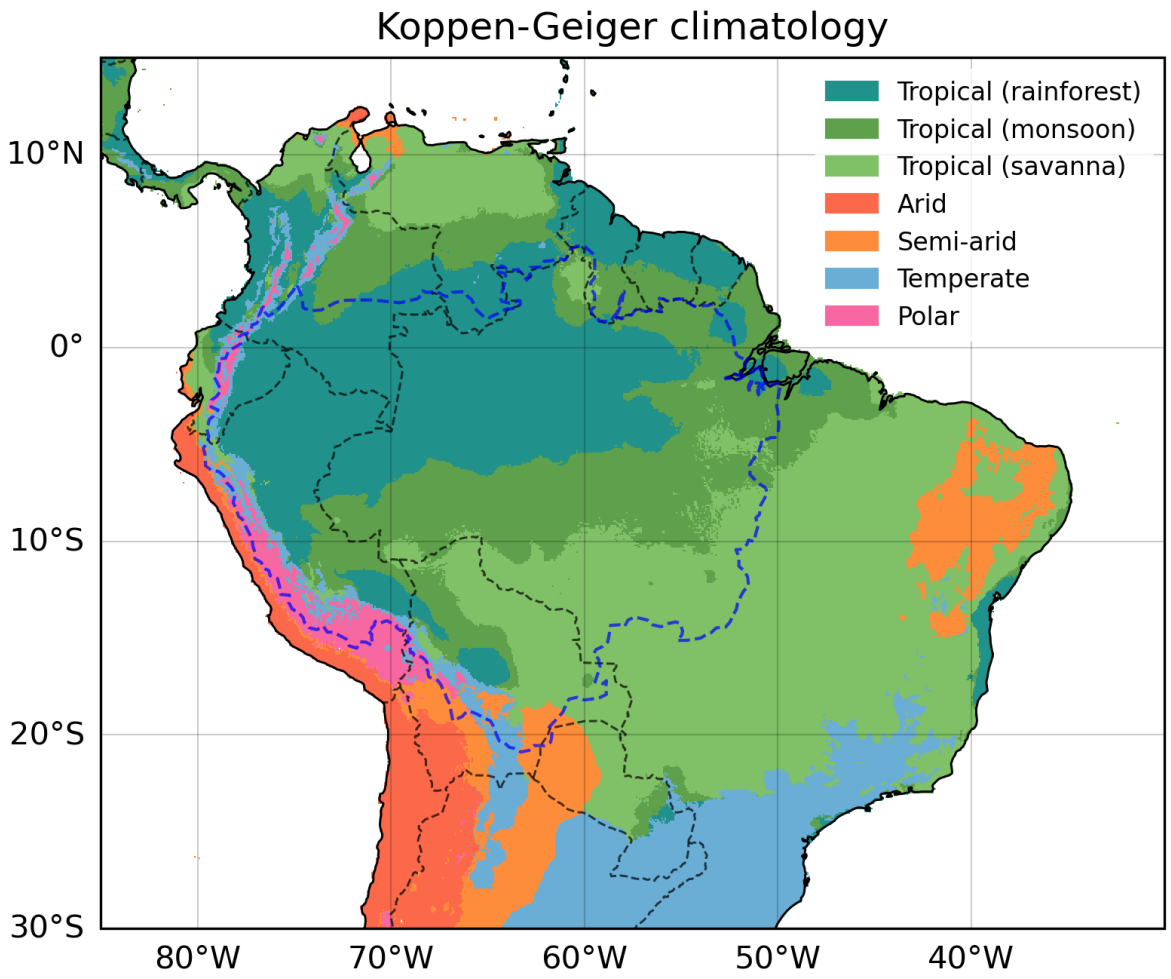

Figure A1: Koppen-Geiger climatology for the study region: the Amazon River Basin is highlighted in the dashed blue line.

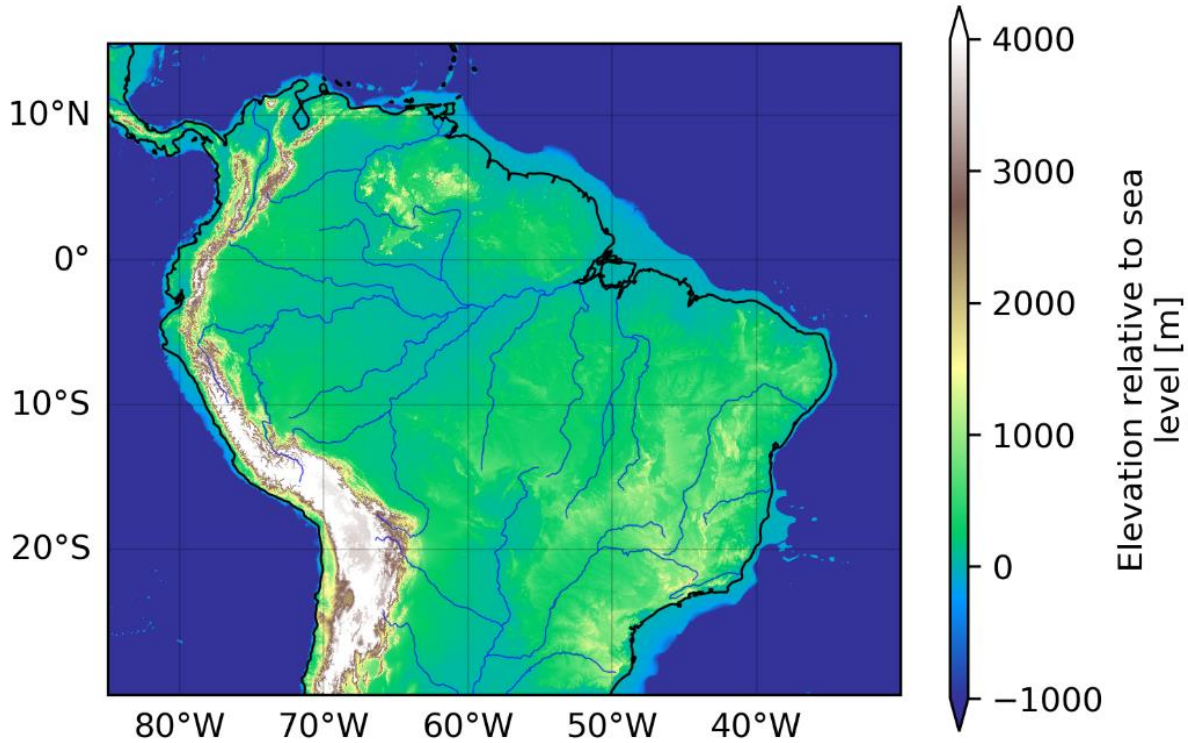

Figure A2: Elevation map of the wider study region relative to sea level.

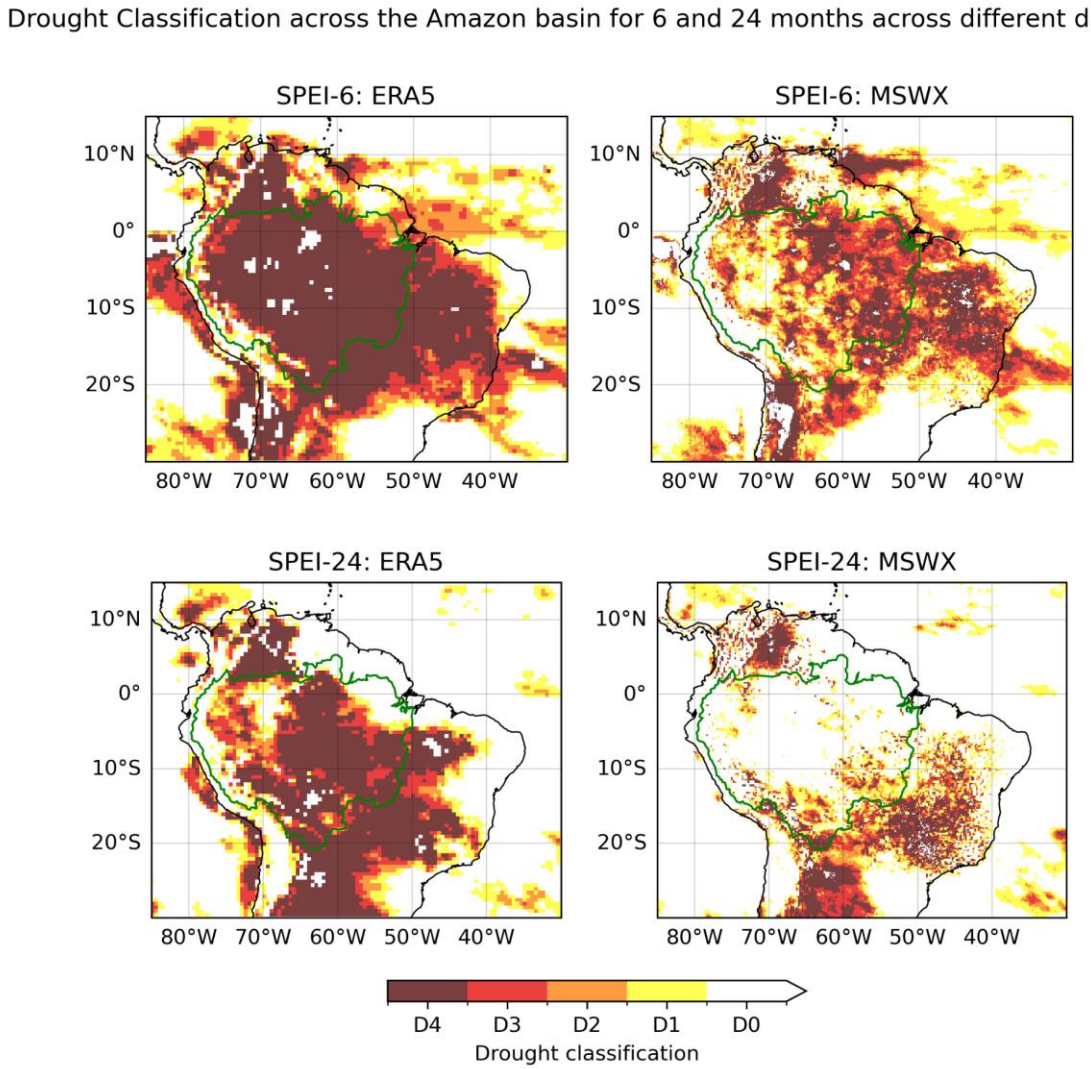

Figure A3: Maps of SPEI-6 and -24 calculated using ERA5 (left panels) and MSWEP/MSWX (right panels, with the Amazon River Basin highlighted in green. The drought is classified according to the US Global Drought Monitor drought classifications (D0 - abnormally dry, D1 - moderate, D2 - severe, D3 - extreme, and D4 - exceptional).

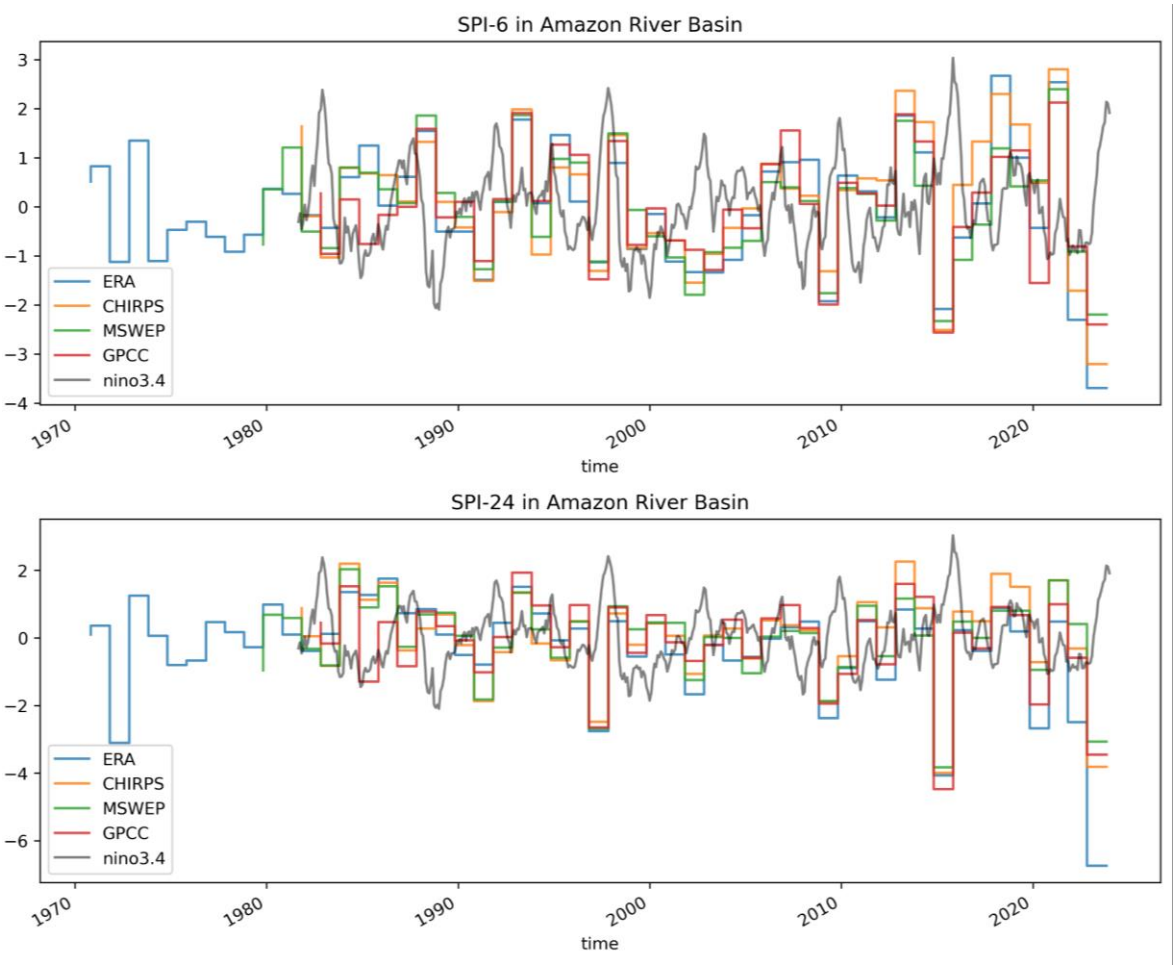

Figure A4: SPI-6 and -24 for the Amazon River Basin calculated using observational datasets ERA5, CHIRPS, MSWEP, GPCC. The Niño*3.4 metric is displayed in black.*

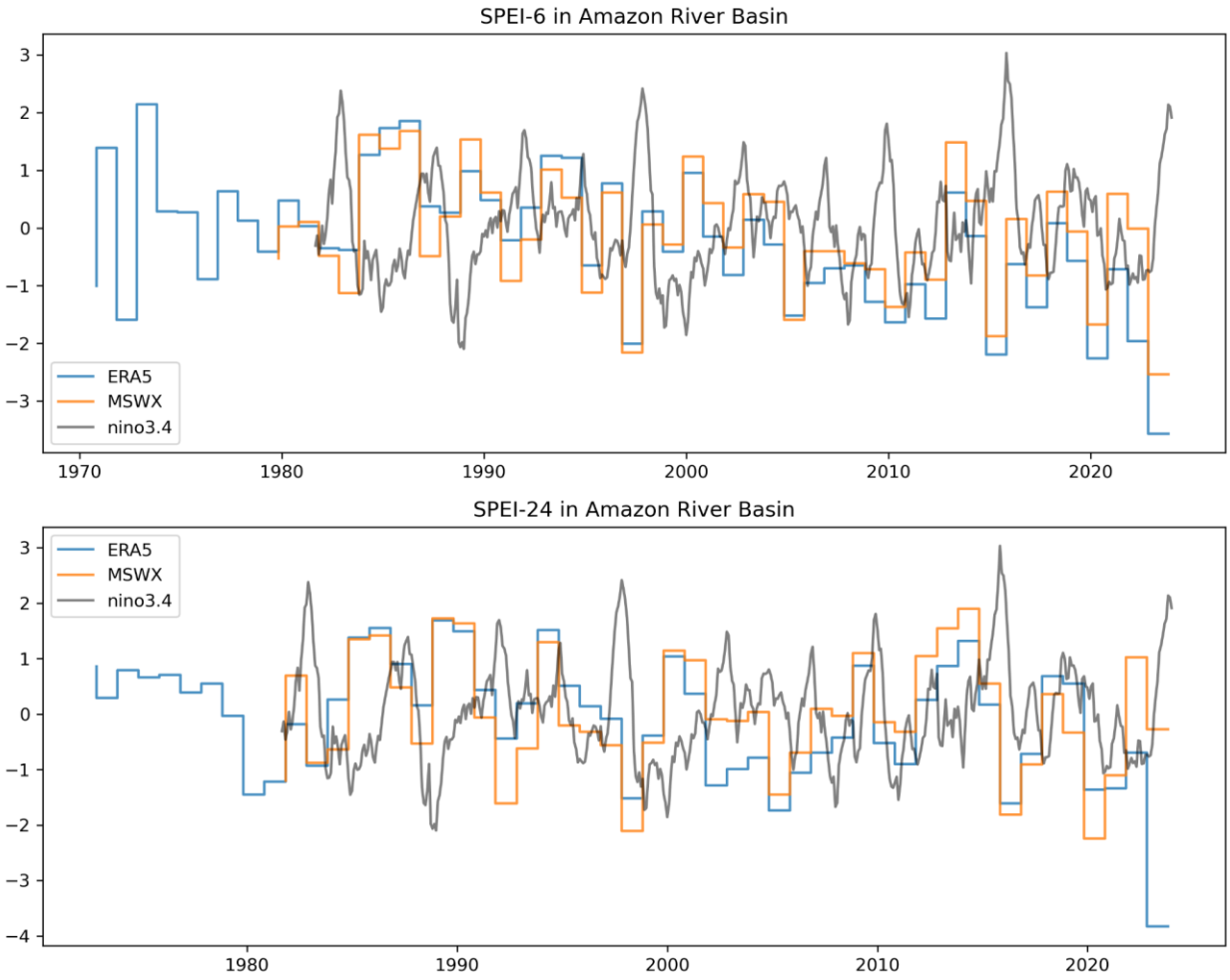

Figure A5: SPEI-6 and -24 for the Amazon River Basin calculated using observational datasets ERA5, CHIRPS, MSWEP, GPCC. The Niño*3.4 metric is displayed in black.*

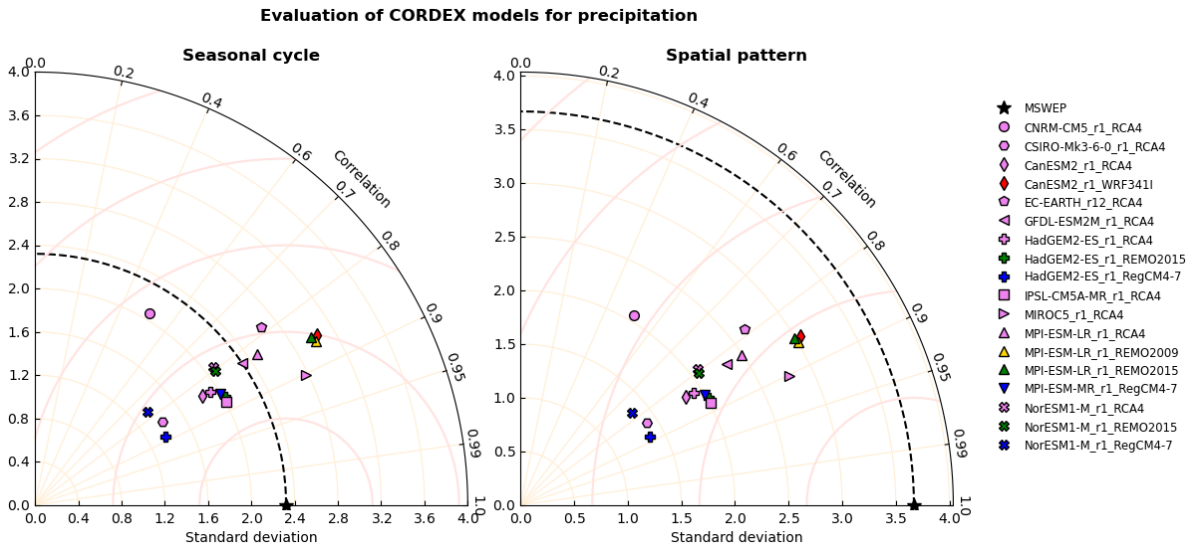

Figure A6: Taylor diagrams used to evaluate seasonal cycle and spatial patterns of precipitation over the Amazon basin in the CORDEX ensemble against the MSWEP reference. The azimuthal angle corresponds to the Pearson correlation coefficient between the simulated climatology and the reference climatology, which quantifies how well the two patterns match; the radial distance from the origin indicates the standard deviation, which measures the amplitude of the pattern.

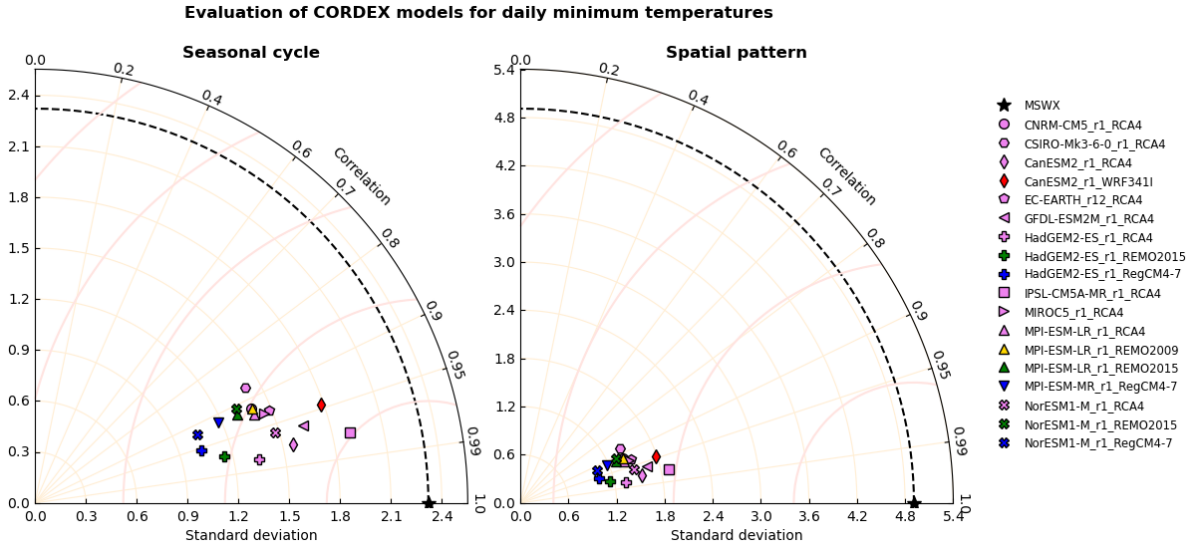

Figure A7: Taylor diagrams used to evaluate seasonal cycle and spatial patterns of daily minimum temperatures over the Amazon basin in the CORDEX ensemble against the MSWX reference. The azimuthal angle corresponds to the Pearson correlation coefficient between the simulated climatology and the reference climatology, which quantifies how well the two patterns match; the radial distance from the origin indicates the standard deviation, which measures the amplitude of the pattern.

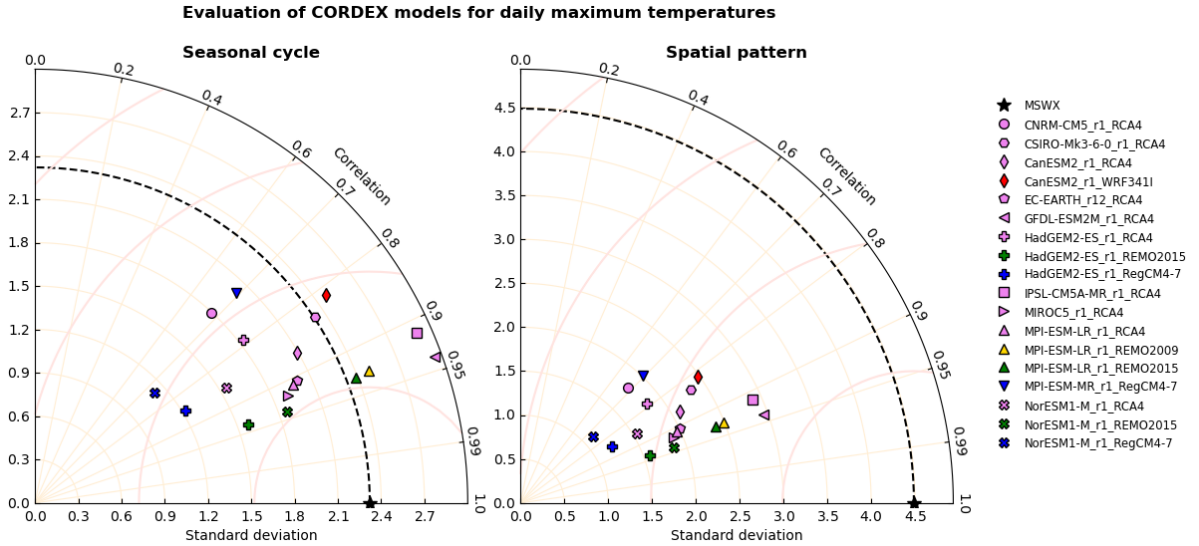

Figure A8: Taylor diagrams used to evaluate seasonal cycle and spatial patterns of daily maximum temperatures over the Amazon basin in the CORDEX ensemble against the MSWX reference. The azimuthal angle corresponds to the Pearson correlation coefficient between the simulated climatology and the reference climatology, which quantifies how well the two patterns match; the radial distance from the origin indicates the standard deviation, which measures the amplitude of the pattern.

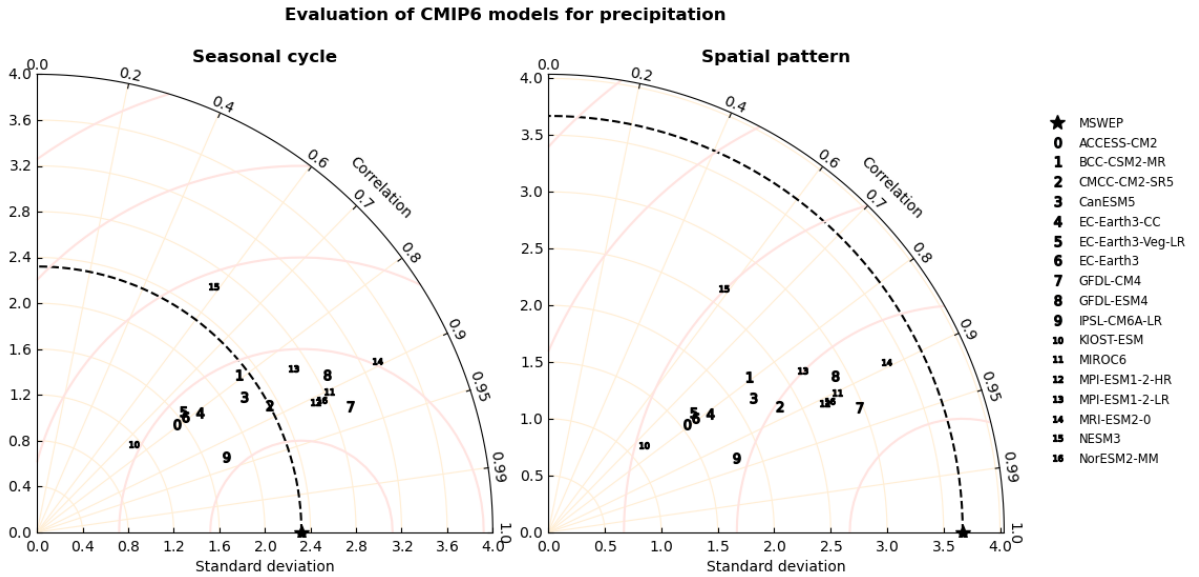

Figure A9: Taylor diagrams used to evaluate seasonal cycle and spatial patterns of precipitation over the Amazon basin in the CMIP6 ensemble against the MSWEP reference. The azimuthal angle corresponds to the Pearson correlation coefficient between the simulated climatology and the reference climatology, which quantifies how well the two patterns match; the radial distance from the origin indicates the standard deviation, which measures the amplitude of the pattern.

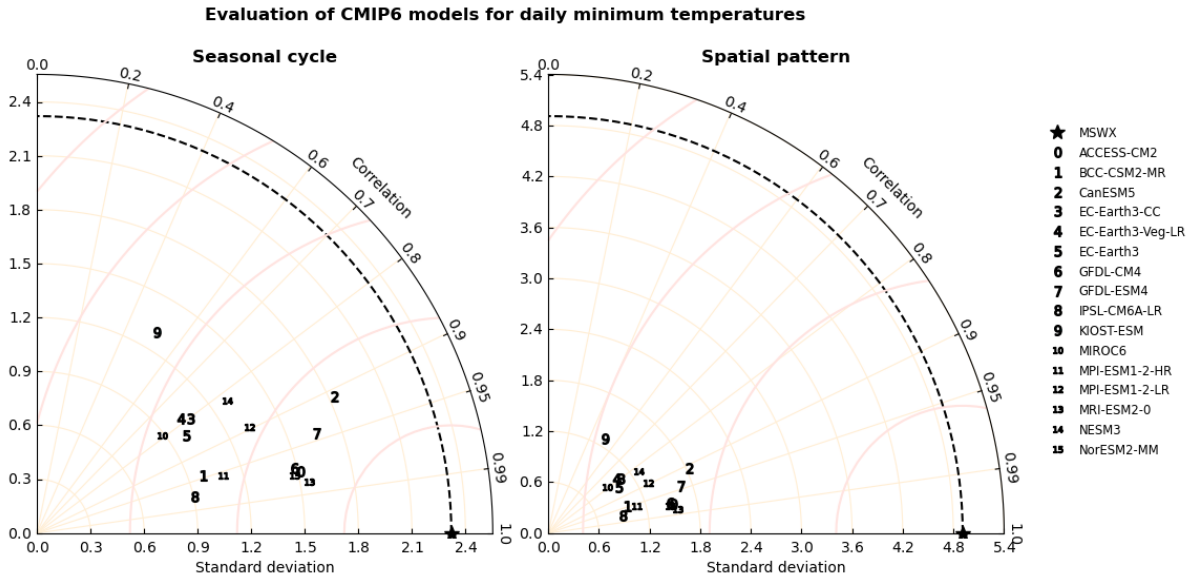

Figure A10: Taylor diagrams used to evaluate seasonal cycle and spatial patterns of daily minimum temperatures over the Amazon basin in the CMIP6 ensemble against the MSWX reference. The azimuthal angle corresponds to the Pearson correlation coefficient between the simulated climatology and the reference climatology, which quantifies how well the two patterns match; the radial distance from the origin indicates the standard deviation, which measures the amplitude of the pattern.

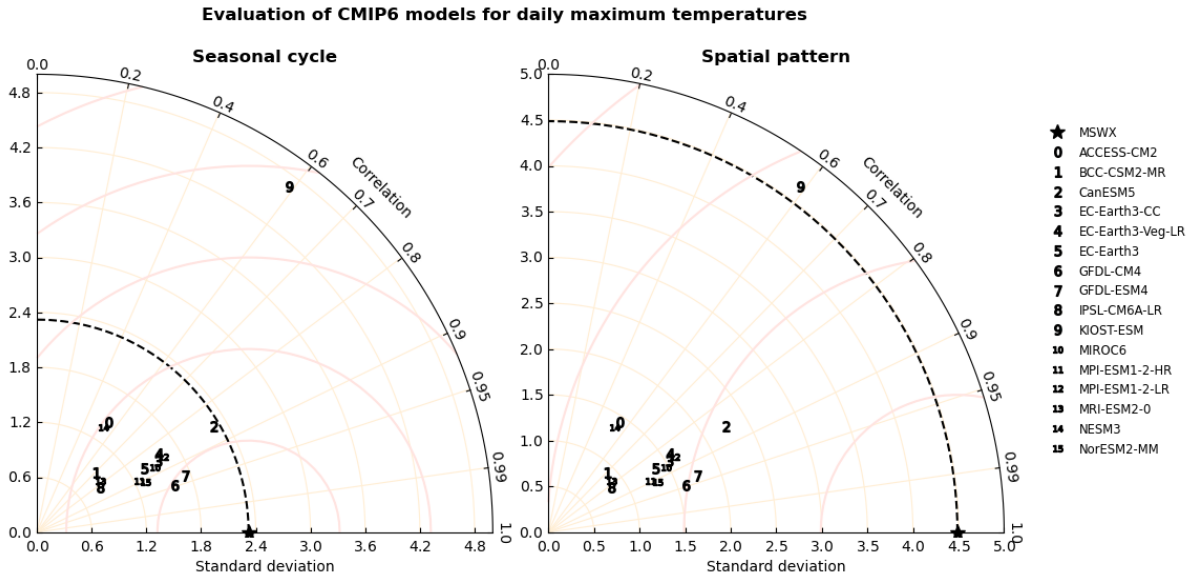

Figure A11: Taylor diagrams used to evaluate seasonal cycle and spatial patterns of daily maximum temperatures over the Amazon basin in the CMIP6 ensemble against the MSWX reference. The azimuthal angle corresponds to the Pearson correlation coefficient between the simulated climatology and the reference climatology, which quantifies how well the two patterns match; the radial distance from the origin indicates the standard deviation, which measures the amplitude of the pattern.